Graphene and graphite nanoribbons: Morphology, properties, synthesis, defects and applications

Article *in* Nano Today · August 2010

DOI: 10.1016/j.nantod.2010.06.010

CITATIONS
296

READS
1,097

11 authors, including:

Andrés Rafael Botello-Méndez
University of Cambridge
38 PUBLICATIONS **1,737** CITATIONS
SEE PROFILE

Yadira I. Vega-Cantu
Tecnológico de Monterrey
16 PUBLICATIONS **741** CITATIONS
SEE PROFILE

Emilio Munoz-Sandoval
Instituto Potosino de Investigación Científica …
72 PUBLICATIONS **1,748** CITATIONS
SEE PROFILE

Jean-Christophe Charlier
Université Catholique de Louvain
214 PUBLICATIONS **12,751** CITATIONS
SEE PROFILE

Nano Today (2010) 5, 351—372

available at www.sciencedirect.com

ScienceDirect

journal homepage: www.elsevier.com/locate/nanotoday

REVIEW

Graphene and graphite nanoribbons: Morphology, properties, synthesis, defects and applications

Mauricio Terrones[a,*], Andrés R. Botello-Méndez[b], Jessica Campos-Delgado[c], Florentino López-Urías[d], Yadira I. Vega-Cantú[d], Fernando J. Rodríguez-Macías[d], Ana Laura Elías[e], Emilio Muñoz-Sandoval[d], Abraham G. Cano-Márquez[d], Jean-Christophe Charlier[b], Humberto Terrones[b]

[a] *Department of Materials Science and Engineering & Chemical Engineering, Polytechnic School, Carlos III University of Madrid, Avenida Universidad 30, Edificio Betancourt, 28911 Leganés, Madrid, Spain*
[b] *Institute of Condensed Matter and Nanosciences (IMCN), Université Catholique de Louvain, Place Croix du Sud 1, B-1348 Louvain-la-Neuve, Belgium*
[c] *Divisão de Metrologia de Materiais, Instituto Nacional de Metrologia, Normalização e Qualidade Industrial (INMETRO), Duque de Caxias, RJ 25250-020, Brazil*
[d] *Advanced Materials Department, IPICYT, Camino a la Presa San José 2055, Col. Lomas 4a sección, 78216, San Luis Potosí, SLP, Mexico*
[e] *Department of Mechanical Engineering and Materials Science, Rice University, Houston, TX 77005, USA*

Received 16 May 2010; received in revised form 26 June 2010; accepted 28 June 2010
Available online 2 August 2010

KEYWORDS
Graphene;
Nanoribbons;
Nanotubes;
Synthesis;
Properties;
Applications

Summary Carbon is a unique and very versatile element which is capable of forming different architectures at the nanoscale. Over the last 20 years, new members of the carbon nanostructure family arose, and more are coming. This review provides a brief overview on carbon nanostructures ranging from C_{60} to graphene, passing through carbon nanotubes. It provides the reader with important definitions in carbon nanoscience and concentrates on novel one- and two-dimensional layered carbon (sp^2 hybridized), including graphene and nanoribbons. This account presents the latest advances in their synthesis and characterization, and discusses new perspectives of tailoring their electronic, chemical, mechanical and magnetic properties based on defect control engineering. It is foreseen that some of the structures discussed in the review will have important applications in areas related to electronics, spintronics, composites, medicine and many others.

* Corresponding author. Tel.: +34 91 624 9447; fax: +34 91 624 9430.
E-mail address: mtterrones@gmail.com (M. Terrones).

1748-0132/$ — see front matter © 2010 Elsevier Ltd. All rights reserved.
doi:10.1016/j.nantod.2010.06.010

Introduction

The discovery of C_{60} Buckminsterfullerene, a beautiful cage-like carbon molecule of 7 Å in diameter (Fig. 1a) [1], stimulated the creativity and imagination of scientists and paved the way to a whole new chemistry and physics of nanocarbons (Fig. 1) [2–4]. Soon after, carbon nanostructures related papers started to increase in number almost exponentially. However, it is important to note that 5 years earlier (1980), Sumio Iijima first reported electron microscope images of nested carbon nanocages (also known as graphitic onions) when studying amorphous carbon films prepared by thermal vacuum deposition. In 1988, Kroto and McKay proposed that such graphitic onions observed by Iijima consisted of nested icosahedral Fullerenes ($C_{60}@C_{240}@C_{540}@C_{960}$.) containing only pentagonal and hexagonal carbon rings (Fig. 1b) [5]. In 1992, Daniel Ugarte observed the reconstruction of polyhedral graphitic particles (nested giant fullerenes) into almost spherical carbon onions [6], due to high-energy electron irradiation inside a high-resolution transmission electron microscope (HRTEM). Similarly, Chuvilin et al. have recently observed the creation of defects on graphene and the eventual formation of C_{60} upon electron irradiation in a HRTEM [7].

Regarding tubular graphene (rolled graphene sheets known as nanotubes), Endo, and coworkers appear to be the first to report the existence of thin single and multi-walled graphitic nanotubes (SWCNTs and MWCNTs) (Fig. 1c) using HRTEM. These nanotubes were produced using a modified chemical vapor deposition (CVD) method used to produce carbon fibers [8], but this 1976 paper did not have a broad impact at that time. The study of carbon nanotubes (CNTs) started in earnest when Sumio Iijima confirmed in 1991 [9], using electron diffraction, that the structure of MWCNTs consisted of nested graphene tubules exhibiting fullerene-like caps [10]. He termed these structures ''graphite microtubules''. They were produced via an arc-discharge between graphite electrodes in an inert atmosphere (no metal catalyst was used); the same method for producing fullerenes [9]. The synthesis of SWCNTs was reported a couple of years later, in 1993, by Iijima's group [11] and Bethune's group [12] using a carbon arc in conjunction with metal catalysts. Soon after, other graphitic nanostructures were successfully produced, including: nanocones (Fig. 1d) [13], peapods [14], nanohorns (Fig. 1d) [15], carbon rings or toroids (Fig. 1e) [16]. More recently, the two-dimensional crystalline allotrope of carbon, called graphene (Fig. 1f), was isolated using the so-called ''scotch-tape method'', where an ingenious method for its observation under an optical microscope was described [17]. As in the case of CNTs, previous works reporting graphene from the reduction of graphene oxide [18] and torn from graphite with an

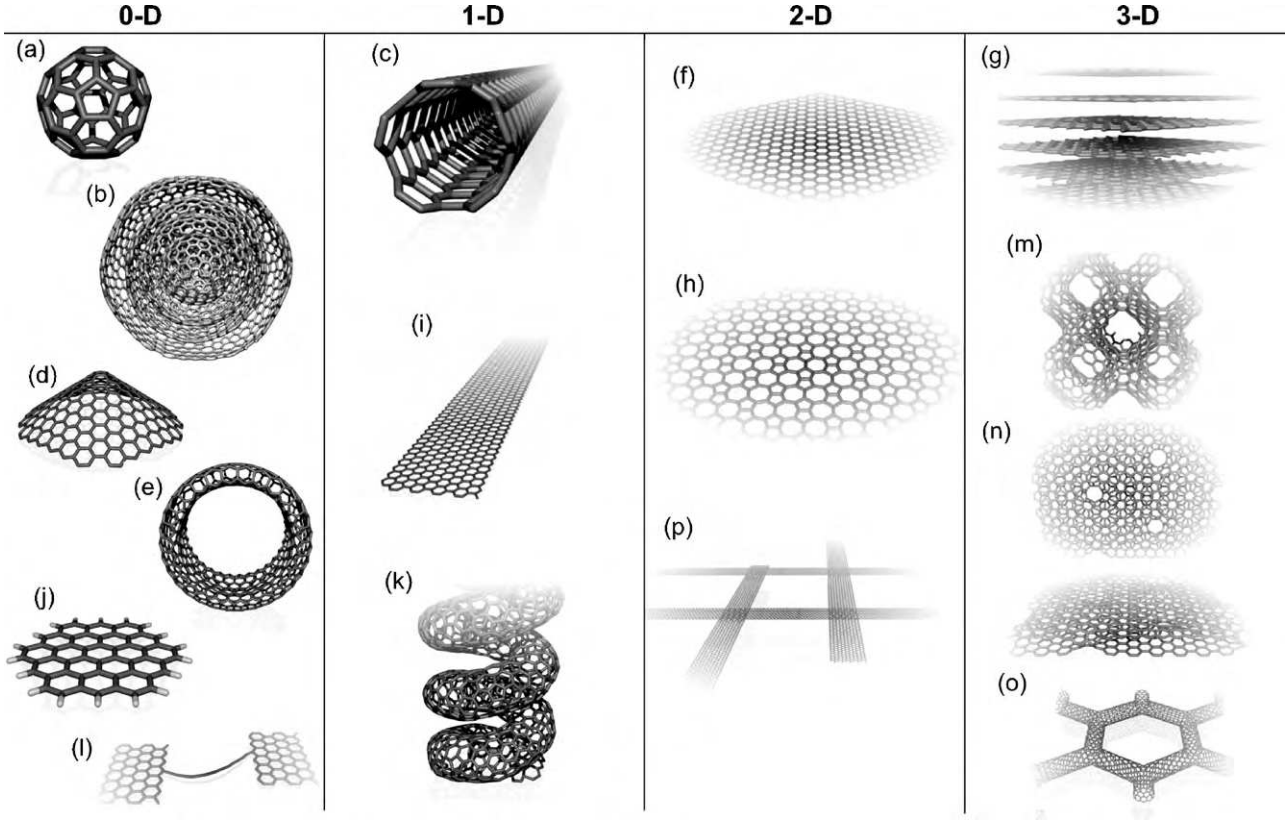

Figure 1 Molecular models of different types of sp^2-like hybridized carbon nanostructures exhibiting different dimensionalities, 0D, 1D, 2D and 3D: (a) C_{60}: Buckminsterfullerene; (b) nested giant fullerenes or graphitic onions; (c) carbon nanotube; (d) nanocones or nanohorns; (e) nanotoroids; (f) graphene surface; (g) 3D graphite crystal; (h) Haeckelite surface; (i) graphene nanoribbons; (j) graphene clusters; (k) helicoidal carbon nanotube; (l) short carbon chains; (m) 3D Schwarzite crystals; (n) carbon nanofoams (interconnected graphene surfaces with channels); (o) 3D nanotube networks, and (p) nanoribbons 2D networks.

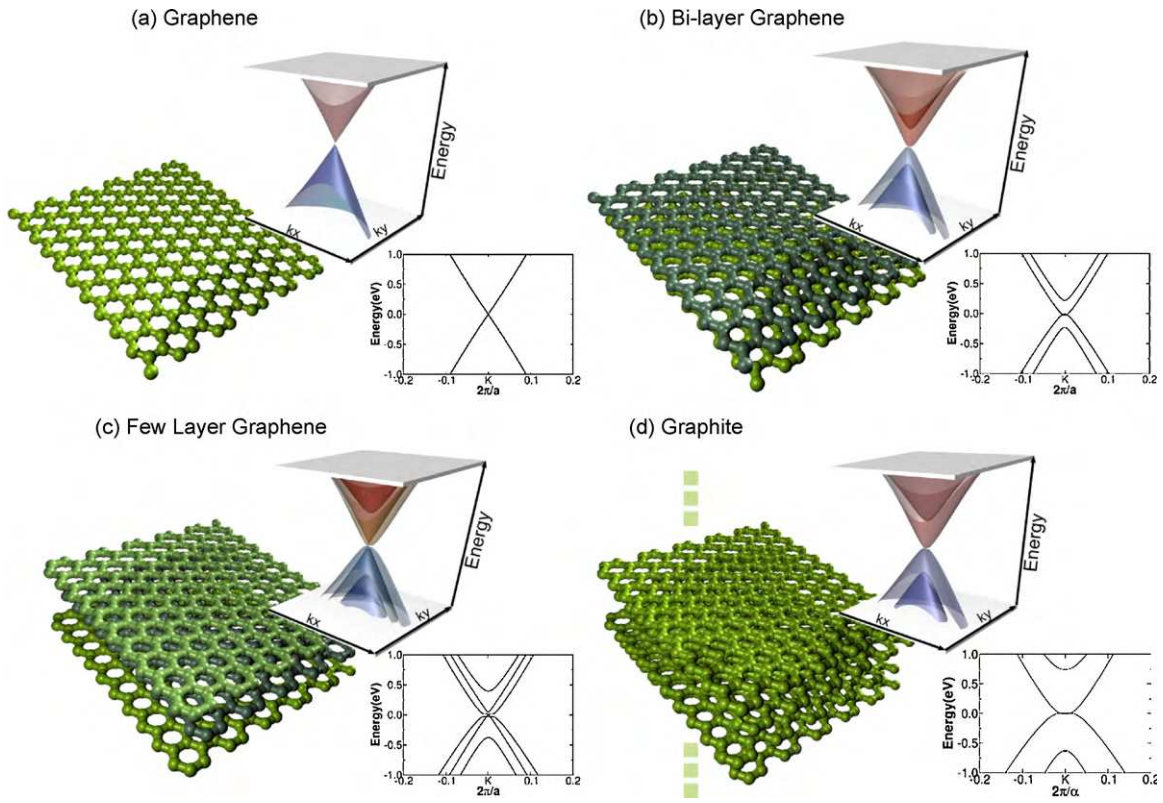

Figure 2 Low energy DFT 3D band structure and its projection on kx close to *k* point K (π/a*[2/3, 0.0 0.0]) for (a) graphene, (b) bilayer graphene, (c) trilayer graphene and (d) graphite. (a) shows the characteristic Dirac point of graphene. The Dirac point (i.e., relativistic fermion characteristic) is lost in bilayer graphene (b), but appears again in trilayer graphene (c); (d) shows the 3D graphite structure which displays a semimetallic band structure with parabolic-like bands. The Fermi level has been set at zero in all cases.

STM tip [19] appeared ahead of its time and did not receive much attention. The relatively easy production of graphene using Novoselov's method, and the peculiar properties of this 2D atomic crystal have heavily stimulated an extensive study of graphene for the first time. New carbon structures with sp^2 hybridization, such as bilayer and few-layer graphene, graphene and graphitic nanoribbons have subsequently emerged, each with novel and unusual properties (Fig. 2).

The series of events described above clearly demonstrate that carbon is a fascinating element and is able to form various morphologies at the nanoscale, possessing different physicochemical properties, some of them yet unknown. There are several reviews and dedicated journal issues on the synthesis and properties of graphene (see, for instance [20,21]). However, the other sp^2 hybridized carbon structures that have emerged from the study of graphene deserve as much of attention as graphene. This review intends to summarize the latest theoretical and experimental advances related to novel one- and two-dimensional layered carbon (sp^2 hybridized).

The different types of graphene-like nanostructures

By looking at the different morphologies of graphene-based nanostructures discovered so far, and all other possibilities still to be found, it is important to provide some important definitions related to different sp^2-like hybridized nanocarbons. In this manuscript the following definitions regarding graphene-like structures will be used:

Graphite: A 3D system

We can define graphite as an infinite three-dimensional crystal made of stacked layers consisting of sp^2 hybridized carbon atoms (Fig. 1g); each carbon atom is connected to other three making an angle of 120° with a bond length of 1.42 Å. Depending on the layers stacking, these crystals could be hexagonal (ABABAB...) or rhombohedral (ABCABC...). The hexagonal and rhombohedal structures belong to the $P6_3/mmc$ (194) and R-3m (166) space groups, respectively. In both 3D crystals, the layers interact weakly through van der Waals forces. Graphite crystals can be found naturally, and can also be artificially synthesized by thermolytic processes; such as the production of highly oriented pyrolytic graphite (HOPG).

Graphene: A 2D system

A graphene crystal is an infinite two-dimensional layer consisting of sp^2 hybridized carbon atoms (Fig. 1f), which belongs to one of the five 2D Bravais lattices called the hexagonal (triangular) lattice. It is noteworthy that by pil-

ing up graphene layers, in an ordered way, one can form 3D graphite. Graphene was initially considered as a theoretical building block used to describe the graphite crystal, and to study the formation of carbon nanotubes (rolled graphene sheets), and predict their fascinating electronic properties. This 2D atomic (one atom thick) crystal of carbon has as fingerprint a unique electronic structure with linear dispersion close to the Fermi level. Charge carriers in graphene are better described as massless Dirac fermions, which result in new phenomena.

There are other pseudo-2D sp^2 hybridized carbon structures, such as bilayer- and few-layer-graphene, which exhibit particular properties that are different from both graphene and graphite (Fig. 2). Whenever these structures exhibit AB stacking they will be referred as graphitic stacks. This distinction is made because it has been demonstrated that the properties of graphene can be recovered in systems with several sp^2 hybridized carbon layers when stacking disorder is introduced. However, the physicochemical properties of graphene appear to be very different from bilayer graphene and few-layer graphene. Therefore, it is also important to include these two graphene categories in this review (see below and Fig. 2).

Theoretical work has been proposed regarding the possibility of stable flat sp^2 hybridized carbon sheets containing pentagons, heptagons and hexagons, termed Pentaheptite (2D sheets possessing heptagons and pentagons only) [22] or Haeckelites (2D crystals containing pentagons, heptagons and/or hexagons: Fig. 1h) [23]. These flat structures are intrinsically metallic and could exist in damaged or irradiated graphene. However, further experiments are needed in order to produce them and identify them successfully.

Some synthesis routes to graphene started to be reported in 2001, using heat treatments, at 1600 °C of diamond nanoparticles over HOPG [24]. However, extensive studies on graphene started only after Novoselov et al. [17] were able to isolate graphene sheets using a simple micromechanical exfoliation method placing scotch-tape over commercial HOPG. The latter technique allowed scientists all over the world to isolate single- and double-layered graphene flakes (SLG and DLG). Subsequently, other methods to obtain graphene flakes were reported, including its epitaxial growth over SiC substrates [25], and CVD growth over thin metal layers [26,27].

Graphene nanoribbons and graphitic clusters: 1D and 0D systems

When infinite graphene crystals become finite, surface and boundaries appear, forming non-three coordinated atoms at the edges, and if the size is in the order of nanometers, we have a graphitic nanostructure that exhibits different properties from those observed in bulk. Among these graphitic nanostructures are nanoribbons (Fig. 1i) and nanoclusters (Fig. 1j). In analogy with the 2D counterpart, one can have graphene-, bilayer-, few-layer- and graphitic-nanoribbons or nanoclusters. It is noteworthy that fullerenes (Fig. 1a and b), graphitic nanotubes (Fig. 1c) and related structures, such as toroids (Fig. 1e) and carbon helixes (Fig. 1k) can be treated as separated systems since bending needs to be considered and curvature effects play an important role. In general, a graphitic (graphite or graphene) nanoribbon could be defined as a one-dimensional sp^2 hybridized carbon crystal with boundaries that expose non-three coordinated carbon atoms, and possesses a large aspect ratio (Fig. 1i). Edge terminations could be armchair, zigzag or a combination of both. The graphitic cluster concept arises when the dimensionality is lost and no periodicity is present (Fig. 1j). Finally, long carbon chains with alternating (single—double) bonds, could be considered as 1D system, and such systems have been investigated experimentally and theoretically [28]. If these chains become small or finite, the system could be considered as a 0D (Fig. 1l) [29]. In both cases, these chains are fascinating and further experimental work needs to be performed.

Schwarzites and nanotube networks: Curved graphene in 3D

Schwarzites are hypothetical graphitic (sp^2 hybridized) three-dimensional crystals obtained by embedding non-hexagonal carbon rings (Fig. 1m), thus spanning to different space groups, in which the most symmetrical cases belong to cubic Bravais lattices [30]. These structures could be visualized as microporous carbon (Fig. 1n), exhibiting nanochannels. It is important to note that similar structures have been synthesized. In this context, the use of mesoporous silicates as templates to introduce a carbon source (e.g. sucrose), followed by a carbonization and an HF treatment yield microporous carbon in which small regions can be compared and explained with the structure of Schwarzites [31,32]. From the theoretical standpoint, these mesoporous carbon materials have been predicted to have outstanding performance in the storage of hydrogen due to their large surface area [33], however further attempts to improve their storage capacity need to be carried out [34]. Another type of 3D array of nanocarbons, consists of nanotube networks (Fig. 1o), which have been predicted to exhibit outstanding mechanical and electronic properties, besides having a large surface area (e.g. 3600 m^2/g) [35,36]. Interestingly, these type of random 3D nanotube networks have been produced using CVD approaches [37,38] and further theoretical and experimental studies are still needed in order to achieve crystalline 3D networks.

Properties

Properties of graphene and few-layered graphene

The crystal structure of graphene can be thought of as two equivalent carbon triangular sub-lattices. Due to symmetry considerations, the hopping of electrons between the sub-lattices leads to the formation of two energy bands, which intersect at the *K* point (Fig. 2a) [39]. Near these crossing points, the electron energy is linearly dependent on the wave vector. This linear dispersion results in massless excitons, which are described by the Dirac equation. Dirac fermions (electrons or holes) exhibit very different and unusual properties compared to ordinary electrons, thus leading to new phenomena. For instance, the anomalous integer quantum Hall effect can be observed in graphene even at room temperature [40,41]. Other outstanding properties of graphene include insensitivity to

external electrostatic potentials (Klein paradox), jittery motion of the wave function under confining potentials, and large mean free paths. For a comprehensive review of the properties of graphene, see Ref. [21].

The electronic properties of graphene change with the number of layers and by the relative position of atoms in adjacent layers (stacking order). For bilayer graphene, the stacking order can be either AA, with each atom on top of another atom; or AB, where a set of atoms in the second layer sits on top of the empty center of a hexagon in the first layer. As the number of layers increase, the stacking order can become more complicated. For graphite, there are three common types of stacking: (i) AB or Bernal stacking, (ii) ABC or rhombohedral stacking, and (iii) no discernible stacking order or turbostratic stacking. The most stable stacking is AB, thus it has been studied more than other graphene-based stacks. However, the other stacking orders are certainly possible, especially in few-layer graphenes, and remain to be studied in detail. In fact, it has been recently found that bilayer graphene often exhibits AA stacking [42].

The limit of thickness at which graphene can still be considered as such, can be determined by the rapid change in the electronic structure as the number of layers increase. The first AB stacks of graphene show very different electronic spectra (Fig. 2). The bilayer (Fig. 2b) shows parabolic bands (thus no Dirac electrons), which touch at the Fermi level. Under the presence of an electric field, the gap on bilayer graphene can be opened, which is of interest in technological applications [43]. The trilayer shows an interesting band structure, which looks like a combination of the monolayer and the bilayer. In general, for few-layer graphene with N layers (AB stacking), there will be a linear band (Dirac fermions) if N is odd [44]. As the number of layers increases, the band structure becomes more complicated: several charge carriers appear [17,45], and the conduction and valence bands start notably overlapping [17,46]. Therefore, three different types of pseudo-2D crystals are distinguished: *graphene, and double- and few-layer graphene*. Thicker structures can be considered as thin films or slabs of graphite [20]. The stacking order or disorder has been found to dramatically change the electronic properties of multilayer graphene, introducing Dirac fermions due to symmetry breaking, even in graphite crystals to form graphene stacks [47,48].

The thermal properties of graphene have been recently measured by Balandin, et al. [49], who found that a suspended graphene sheet obtained by mechanical exfoliation could exhibit extremely high thermal conductivity values ranging from $(4.84 \pm 0.44) \times 10^3$ to $(5.30 \pm 0.48) \times 10^3$ W/m K; higher than experimental values for carbon nanotubes and diamond. However, more recent experimental results on CVD grown suspended graphene indicate lower values (~2500 W/m K) [50]. Nevertheless, these outstanding thermal properties could be exploited in the fabrication of heat dissipaters and polymer composites with high thermal conduction. It is important to note that a detailed study regarding the thermal properties of doped-graphene and individual graphene nanoribbons still need to be performed and compared with the data shown above.

Regarding the mechanical strength of an individual graphene sheet, Hone and coworkers [51] have demonstrated that graphene has a breaking strength of 200 times larger than that of steel, with a Young's modulus of ca. 1 TeraPascal (TPa). These measurements appear to depend upon the number and types of defects present within the sheet (see defect section below). In this context, McEuen and coworkers reported [52] using atomic force microcopy, a Young's modulus of 0.5 TPa for an individual graphene sheet. It is noteworthy that the Young's modulus of graphite along the basal plane is *ca.* 1 TPa. To the best of our knowledge, mechanical property measurements of graphene nanoribbons have not been reported hitherto. However, these measurements will be very dependent on the number and types of defects (see below), and type of edge terminations. In addition, one would expect that although doped-graphene nanoribbons may be more chemically active, their mechanical modulus and strength would decrease as the number of dopants increases. However, these sets of experiments are still needed and should be carried out.

The interplay between mechanical and electronic properties of graphene has been recently studied. Kim and coworkers have measured the change of resistance of graphene (grown by CVD on nickel and then transferred to a flexible substrate) upon mechanical strain [27]. When graphene is bent (*ca.* 1 mm of diameter), the resistance (initially *ca.* 300 Ω) in the bent direction increases almost one order of magnitude. Similarly, the resistance changes by stretching, with one order of magnitude difference between the resistance parallel and perpendicular to the stretching direction. Theoretical calculations indicate that uniaxial stress do not change significantly the electronic properties of graphene [53–55], but that anisotropic strain or out of plane deformation due to substrate interactions can open a gap between the valence and conduction bands.

Highly crystalline graphene surfaces appear to be chemically inert, and these surfaces usually interact with other molecules via physical adsorption (π–π interactions). However, several chemical groups such as carboxyl (COOH), carbonyl (COH), hydrogenated (CH) and amines (NH_2), could be anchored at the edges of graphene nanoribbons, which are more chemically reactive. In addition, the chemical reactivity could change drastically at these edges, depending on their carbon termination, either armchair or zigzag. In order to make the graphene surface more chemically reactive, either surface defects or high degrees of curvature need to be introduced (see below).

It is important to emphasize that one way to make the graphene surface less inert is by reacting it with halogen atoms such as fluorine. Fluorinated graphite has been synthesized for decades. However, graphene has been recently been fluorinated using different techniques including plasma treatments, F_2 high temperature treatments among others [56,57]. Fluorinated graphene can be dispersed homogenously in solvents and could therefore be used to produce polymer composites. It is also important to mention that the electronic properties of graphene could be tuned via fluorination, which controls the band gap of the material [58].

Regarding the reactivity of graphene, a fully hydrogenated graphene sheet, termed *''graphane''*, was predicted by Sofo et al. [59], and reported experimentally by Novoselov and coworkers [60]. However, the synthesis of this doped graphane layer still needs to be improved and further analysis related to the C–H bonding nature using X-

ray photoelectron spectroscopy (XPS) should be carried out. For graphene nanoribbons, fluorination and hydrogenation reactions remain to be carried out together with XPS and other studies. Such studies are important for devices as it has been shown that electronic properties of graphene can be changed by passivating its surface followed by desorption of hydrogen in specific patterns [61].

Finally, it is also possible to produce graphene oxide materials by attaching oxygenated groups on the sp^2 hybridized surface (e.g. carbonyl and carboxyl groups), making them hydrophilic and more reactive [62]. This layered oxide is commonly produced via wet chemical methods and could also be dispersed easily in different solvents for fabricating robust polymer composites [63]. Due to the large number of defects contained in this layered material, details and other applications of this type of oxidized graphenes will not be reviewed here, and relevant information could be found elsewhere [63].

Properties of graphitic nanoribbons

As explained above, graphitic nanoribbons will inevitably have borders which can exhibit edge states and different electronic, chemical and magnetic properties depending on the size and type of border. The most studied chiral edge configurations, 0° (armchair) and 30° (zigzag), lead to armchair and zigzag nanoribbons (A-GNRs, Z-GNRs), respectively. Experimental results indicate that these are the most common type of edges in nanoribbons (Fig. 3) [64], although edge reconstruction with pentagonal and heptagonal carbon rings has also been observed (see [65] and Section 5).

Electronic properties

Z-GNRs exhibit edge states not present in the armchair case [66,67]. These edge states are present as a flat band around the Fermi level, but extended along the ribbon's edge, leading to a metallic nanoribbon if the width is large enough (e.g. >10 nm) [68,69]. Such flat band results in a high density of states located at the edges, indicating that they are very reactive sites. Furthermore, Z-GNRs exhibit magnetic properties that are relevant for spintronics (see below).

The properties of A-GNRs have a characteristic dependence on the width. Density functional theory (DFT) calculations indicate that A-GNRs can be grouped in three families of decreasing band gaps (E_g) as the ribbon width increases. Barone et al. [70] predicted that in order to produce materials with band gaps $E_g \sim 0.7$ eV (similar to Ge or InN), the width of the ribbons must range between 2 and 3 nm. The ribbon widths must be reduced to 1—2 nm if larger band gaps (1.1—1.4 eV, such as Si, InP, or GaAs) are needed [70], and as the width increases the band gap tends to the zero value of 2D graphene. A nice comparison between experimental and calculated band gaps can be found in Ref. [71]. The effect of thickness (i.e., number of stacking layers) has also been studied. According to theoretical studies, Z-GNRs have increased numbers of edge states, and A-GNRs have decreased band gaps, when multilayered [72]. The E_g of a bilayer A-GNR (b-A-GNR), in general, is smaller than that of an A-GNR, b-A-GNR also exhibits two distinct groups, metal and semiconductor, whereas an individual A-GNR displays purely semiconducting behavior. Moreover, E_g of b-A-GNR is highly sensitive to the interplanar distance [73]. Other studies have shown that A-GNRs exhibit three classes of bilayer gaps, which decrease with increasing ribbon width [74].

Edges in graphene and few-layer graphene nanoribbons have highly reactive sites. Thus, the modulation of the electrical, chemical and magnetic properties of graphene, and multilayer graphene nanoribbons, by anchoring different atoms or molecules on its edges, has been proposed for applications such as sensors, memory devices and processing

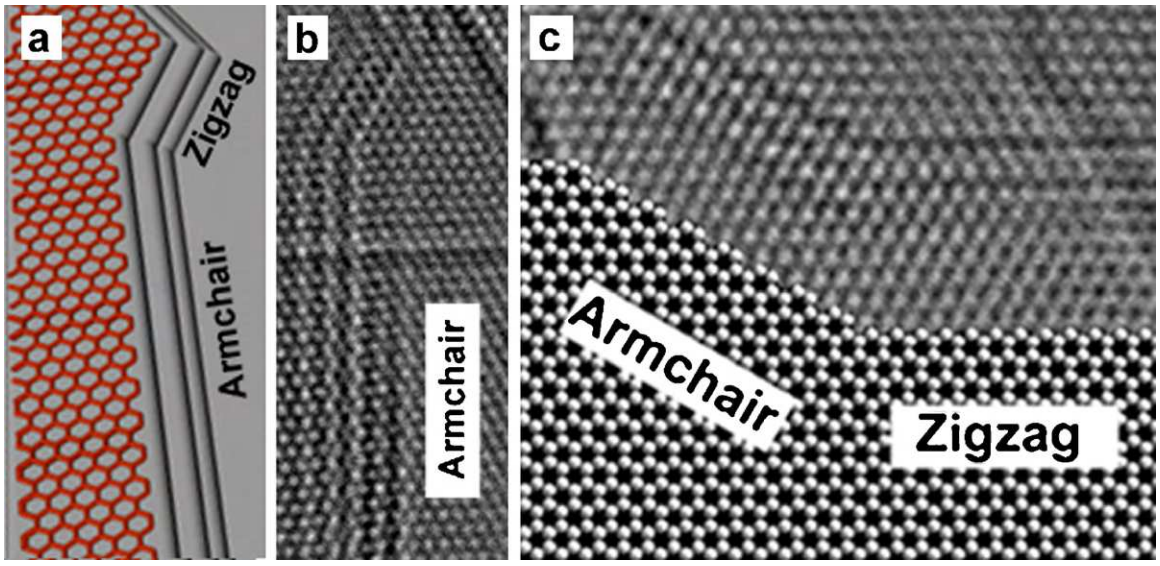

Figure 3 (a) Model of a graphene nanoribbon edge showing an armchair and a zigzag junction (courtesy of M. Hofmann and X. Jia); (b) HRTEM image of graphene edges exhibiting overlapping armchair edges (like terraces of graphene layers with armchair morphology) together with zigzag edges; the image was obtained after applying Joule heating to a graphitic ribbon and resembles the model shown in (a), and (c) HRTEM image of 3 overlapping zigzag-armchair edges obtained by applying Joule heating to a graphitic nanoribbon inside a HRTEM; hexagonal models are depicted for clarity [64].

devices [75—77]. In addition, it has been found that the electronic properties, and in particular the band gap of few-layer graphene is strongly modulated by the interlayer distance. This effect could be used for nano-electromechanical systems (NEMS) [78]. Similarly, strain can induce changes in the electronic properties of graphene nanoribbons. Theoretical calculations indicate that uniaxial strain [79] and out of plane deformations can change the band gap of A-GNRs [80,81].

Quantum transport in graphene nanoribbons

In contrast to carbon nanotubes, quantum transport properties of GNRs are expected to strongly depend on whether their edges exhibit the armchair or the zigzag configurations. As discussed above, the electronic properties of GNRs reveal a strong dependence on the edge topology [66].

All A-GNRs are semiconductors with energy gaps which decrease as a function of increasing ribbon widths. According to the convention, A-GNRs Z-GNRs can be classified by the number N of zigzag or C—C dimer lines across the ribbon width, as illustrated in Figs. 4 and 10 [82]. The gap of specific N-aGNRs depend on the N value, separating the ribbons in three different categories (all exhibiting direct band gaps at the Γ point). The calculated quantum conductances of two A-GNRs exhibiting respectively large and small band gaps, are illustrated in Fig. 4. The 16-A-GNR is a $\sim$0.8 eV gap semiconductor, thus inducing a quite large energy interval where no transmission is allowed (Fig. 4a), while the gap of the 17-aGNR is reduced to less than 0.2 eV (Fig. 4b). The region of zero conductance is also reduced accordingly, and a very small external electric field could induce an electronic transmission through one channel ($1G_0$: quantum value of conductance).

Similarly, Z-GNRs also exhibit direct band gaps which decrease when increasing their width. However, in Z-GNRs, quantum transport is dominated by edge states which are expected to be spin-polarized owing to their high degeneracy. Indeed, due to topological reasons, zigzag-shaped edges give rise to specific extended electronic states which decay exponentially inside the graphene sheet [66]. The ground state of Z-GNRs with hydrogen passivated zigzag edges exhibit finite magnetic moments on each edge with negligible change in atomic structure [83], thus demonstrating that Z-GNRs possess half-metallic (i.e., exhibit a band gap for only one kind of spin) properties and suggesting them to be attractive for spintronic applications [84]. Indeed, upon inclusion of the spin degrees of freedom within *ab initio* calculations (LSDA), Z-GNRs are predicted to exhibit a magnetic insulating ground state with ferromagnetic ordering at each zigzag edge, and anti-parallel spin orientation between the two edges [83]. The total energy difference between ferromagnetic ($\uparrow\uparrow$) and antiferromagnetic ($\uparrow\downarrow$) couplings between the edges is of the order of $\sim$20 meV per edge atom for an 8-Z-GNR. However, such energy difference decreases as the width of the ribbon increases and eventually becomes negligible if this width is significantly larger than the decay length of the spin-polarized edge states [85]. Because the interaction between spins on opposite edges increases when decreasing their width, the total energy of an N-Z-GNR with antiferromagnetic arrangement across opposite edges is always lower than that of a ferromagnetic arrangement for low value of N ($N < 30$). The spin-dependent calculations of quantum conductances of an 8-Z-GNR are illustrated in Fig. 4c and d for the two magnetic configurations ($\uparrow\downarrow$ and $\uparrow\uparrow$) of the ribbon edges. The $\uparrow\downarrow$ spin configuration of the 8-Z-GNR preserves the semiconducting behavior of the GNR family, and its electronic transmission function displays a gap of 0.5 eV around the Fermi energy (Fig. 4c). On the contrary, in the $\uparrow\uparrow$ spin configuration, the 8-Z-GNR becomes metallic, inducing a non-zero electronic transmission function at the Fermi energy (Fig. 4d). In addition, the spin-dependent conductance calculation reveals that the transmission of π electrons with one type of spin orientation (*majority*-spin) is favored for an energy region around -0.5 eV, below the charge neutrality point. On the contrary, π^* electrons with the other orientation (*minority*-

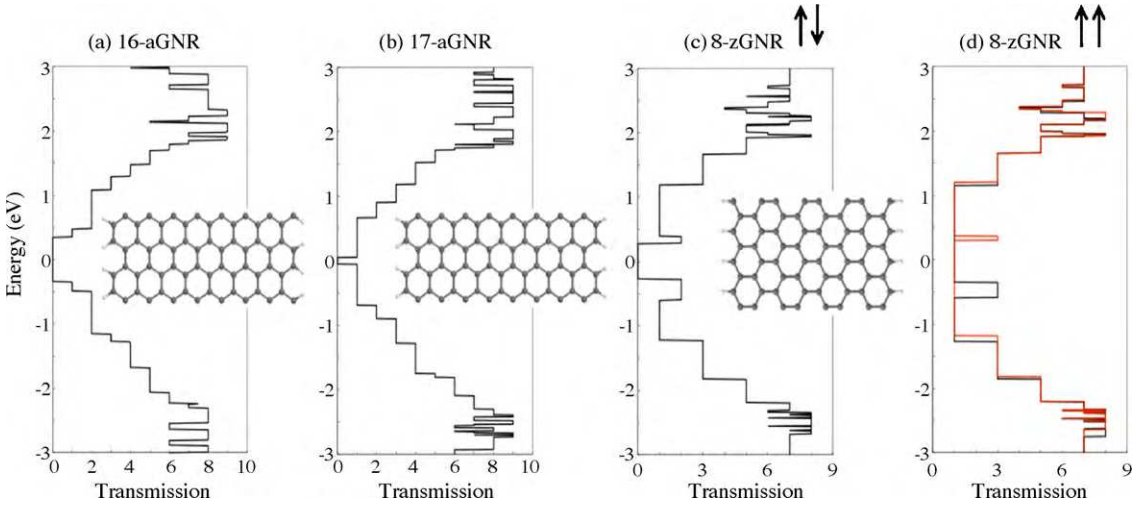

Figure 4 Quantum transport in graphene nanoribbons. Atomic structures and electronic transmission of (a) 16-armchair GNR; (b) 17-armchair GNR, 8-zigzag GNR with (c) anti-parallel $\uparrow\downarrow$ or (d) parallel $\uparrow\uparrow$ spin orientations between the two magnetic edges. The spin-dependent transport is evaluated for both magnetic configurations of the 8-zGNR (c and d) but is only visible for the parallel $\uparrow\uparrow$ spin orientations (ferromagnetic one). In such case, one spin orientation is labeled *majority*-spin (in black) while the other is labeled *minority*-spin (in red). Adapted from Ref. [82].

spin) are more easily transmitted around +0.3 eV above the Fermi energy.

In conclusion, the unusual electronic and transport properties of GNRs indicate that these carbon nanomaterials could be excellent new building blocks in future carbon-based nanoelectronics, thus opening alternatives to the current silicon-based electronics, through the use of new variable states (e.g. quantum states, spin, etc.).

Synthesis of graphitic and graphene nanoribbons

There is a wide spectrum of methods available to produce carbon nanoribbons, from CVD, through chemical treatments of graphite to the unzipping of carbon nanotubes.

Chemical vapor deposition of graphitic nanoribbons

GNRs were first reported in 1990 by Murayama and Maeda [86], from hydrocarbon decomposition or disproportionation of carbon monoxide at 400—700 °C, catalyzed by metal particles generated from $Fe(CO)_5$, in flowing CO/H_2 gas. The typical ribbon-like filaments were 10 μm long, 0.1—0.7 μm wide and 10—200 nm thick, with a catalyst particle at one end (Fig. 5a and b), and graphitic layers with a uniform orientation perpendicular to the filament axis. Annealing treatments at 2800 °C resulted in loop formation at the open edges of graphitic layers. Recent works have confirmed that loop formation between adjacent sheets is a more stable configuration after annealing treatments on graphitic nanostructures at temperatures >1500 °C [87,42].

Another CVD production method of graphitic nanoribbons was reported by Campos-Delgado et al. in 2008 (Fig. 5c and d) [88]. In this work a spray (atomized droplets) of ferrocene in ethanol, with thiophene, carried by Ar to a furnace at 950 °C, produced rippled nanoribbons, several micrometers long, 20—300 nm wide and <15 nm thick. The highly crystalline material had the (0 0 2) planes parallel to the main ribbon axis. Catalytic particles were not found but ribbons did not form if ferrocene or thiophene were not used. Therefore, further studies aiming at understanding their growth should be carried out. High temperature treatments of such nanoribbons improve the degree of crystallinity and promote loop formation at the edges of the graphitic layers [87]. Interestingly, electron beam irradiation combined with

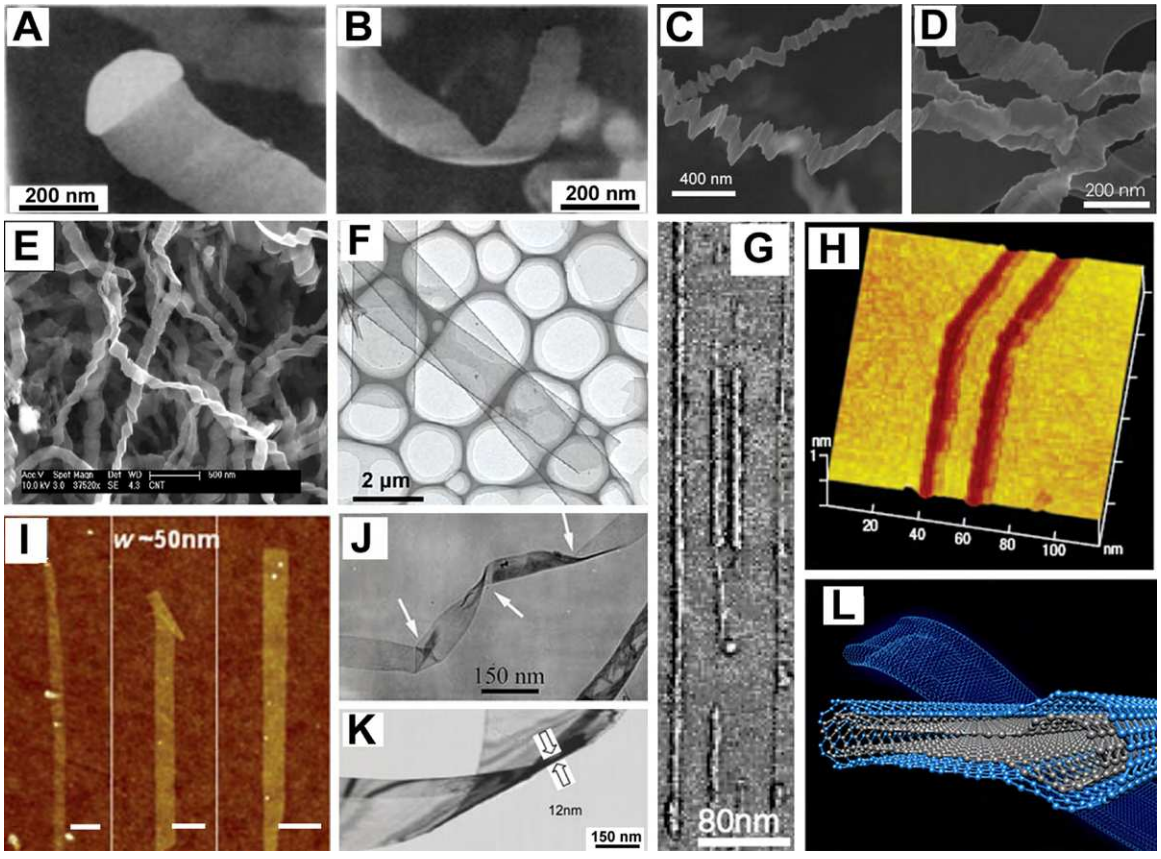

Figure 5 CVD and other production methods of graphitic nanoribbons. (a and b) Scanning electron micrographs of Murayama's filamentous graphite, showing Fe particles at the ends of the structures [86]; (c and d) SEM images of the graphitic nanoribbons produced by pyrolysis of ethanol—ferrocene—thiophene solutions [88]; (e) SEM image of the nanoribbons produced by pyrolysis of THF and ferrocene solutions [89], (f) low magnification TEM image of the nanoribbons produced by the ZnS template method [94], (g) AFM image of the nanoribbons obtained through high temperature treatments of diamond nanoparticles [24], (h) 3D STM image of an 8-nm-wide graphene nanoribbon patterned by STM lithography [95], (i) AFM image of chemically derived nanoribbons from graphite (scale bars = 100 nm) [71], (j and k) TEM images of an amorphous carbon nanoribbon and graphitic nanobelt, respectively, produced by hydrothermal processes [97,98], (l) scheme illustrating the structure of a collapsed nanotube [99—103].

Joule heating experiments inside a HRTEM, resulted in the generation of sharp zigzag and armchair edges (Fig. 3) [64]. This demonstrates that the most stable edges in graphene ribbons are indeed either zigzag or armchair (Fig. 3).

In 2008, Subramanyam, and coworkers reported that pyrolsis of ferrocene and tetrahydrofuran (THF) at 950 °C produced a mixture of crystalline carbon nanoribbons and iron filled MWCNTs (Fig. 5e) [89]. The authors neither specify the relative yield nor the typical dimensions of the produced nanoribbons. By observation of the published images, we estimated them to be ~200 nm in width and tens of microns in length. The crystalline nature of the nanoribbons was confirmed through X-ray powder diffraction, and TEM, with the orientation of the (0 0 2) lattice planes of carbon being perpendicular to the axis of growth.

Chemical vapor deposition of graphene

The precipitation of graphene on metals has been reported by different research groups for over 30 years [90]. More recently, this method has been applied to obtain and study the properties of graphene and few-layer graphene [24–26].

In 2008 Sutter et al. [91] reported the epitaxial precipitation of graphene on Ru(1 1 1) in 2008. In 2009, Rouff et al. [92] reported the large area synthesis of graphene sheets on Cu foil. This article included the development of a transfer technique that could be used to place the grown graphene on another substrate. The transfer process involved the dissolution of the metal foil assisted by an iron nitrate solution.

Reina et al. [26] reported the growth of few-layer graphene on Ni films, by CVD at atmospheric pressure. After some months the same group induced graphene precipitation on annealed polycrystalline Ni surfaces [93]. Large area, single and bilayer graphene sheets were obtained by this method, in which CH_4 was pyrolyzed at 1000 °C. Subsequently, poly(methyl methacrylate) (PMMA) was spin coated on the synthesized graphene surfaces and a wet-etching treatment with HCl dissolved the metal [93]. PMMA served as a support for the free standing graphene sheets that could be placed on different substrates, such as microscopy slides or TEM grids [93].

Yu et al. reported the CVD synthesis of few-layer graphene ribbons using ZnS substrates as templates (Fig. 5f) [94]. Decomposition of CH_4 at 750 °C on ZnS templates and further acid treatments to dissolve the ZnS ribbons produced few-layer graphene nanoribbons (FLGNRs) of ~3.4 nm in thickness, 0.5–5 μm in width and several microns in length. The authors claim to be able to control the morphologies of the produced FLGNRs but no details are provided about the edge structure of the nanoribbons.

Chemical synthesis of graphitic nanoribbons

As discussed above, Affoune, et al. were able to obtain graphene by an electrophoretic deposition of diamond nanoparticles on a HOPG substrate followed by heat treatment [24]. Here the diamond nanoparticles were graphitized into layers forming sheets. Three years later, Cançado, et al. were able to use the same method to produce graphene edges and nanoribbons (Fig. 5g). These edges were characterized by Raman spectroscopy [95].

Alternative chemical routes consisting on the exfoliation of commercial expandable graphite, have been more recently used to produce graphene nanoribbons (Fig. 5i) [71]. In particular, the process consisted on exfoliation of 3D graphite by annealing at 1000 °C followed by 30 min sonication in a solution of dichloroethane and a polymer. After centrifugation of the suspension, GNRs remained in the supernatant. The shape and electrical properties of these GNR were thoroughly examined, and FET devices were created.

Small GNRs could also be synthesized by organic chemistry approaches linking tetra- and hexa-phenylbenzenes through the Suzuki–Miyaura reaction [96]. The polyphenylene formed is then subjected to a cyclodehydrogenation reaction with $FeCl_3$ as the oxidant, resulting in ribbons with 6–12 polycyclic aromatic repeating units. These GNR are highly soluble in common organic solvents due to the introduction of branched alkyl side chains. The lengths of these 2D-GNR were found to be 8–12 nm, and they can form aligned monolayers, as well as crystallize from solution by π–π stacking. This report is a true bottom-up approach to thin and short graphene nanoribbons with armchair edges. It remains to be seen whether these or similar chemical reactions can create wider and/or longer GNR or even be harnessed to create branched GNR.

Amorphous carbon ribbons and crystalline graphitic ribbons have also been produced via a hydrothermal process involving Teflon-lined autoclaves. In order to produce amorphous carbon nanoribbons, benzene, sodium and ferrocene were kept in the reactor at 210 °C for 24 h (Fig. 5j) [97]. The crystalline ribbon structures were synthesized using active carbon and polyoxometalates at 160–180 °C for 72 h (Fig. 5k) [98]. Finally, it could also be possible to produce graphene or graphitic nanoribbons by collapsing large diameter carbon nanotubes (Fig. 5l) [99–103]. This way, transport could occur along the coalesced edges, and further experimental studies are required in order to understand the role of the large curvature imposed by the merging of adjacent edges, the reactivity of such highly deformed sp^2 hybridization states, as well as the effects of the chirality on the sealed edges.

Graphitic nanoribbons from nanotubes

Carbon nanotubes are often described as rolled up graphene sheets; therefore, it would seem natural to unroll them to obtain graphene (Fig. 6). Yet it was not until 2009 that the first method to obtain graphitic nanoribbons from nanotubes appeared published [104]. Two more works related to the unzipping of nanotubes appeared 2 weeks later [105,106]. A fourth method, first suggested by Terrones [107] involved the use of metal catalytic particles as nanoscissors, was successfully proved [108], and early this year, it was also demonstrated that nanotubes could be easily unzipped by passing high electrical current inside the microscope [109]. These different methods to unroll or unzip nanotubes are depicted in Fig. 6.

One of the methods, shown in Fig. 6a, relies on the intercalation of lithium in liquid ammonia, followed by acid and thermal exfoliation treatments (Fig. 7). The resulting mate-

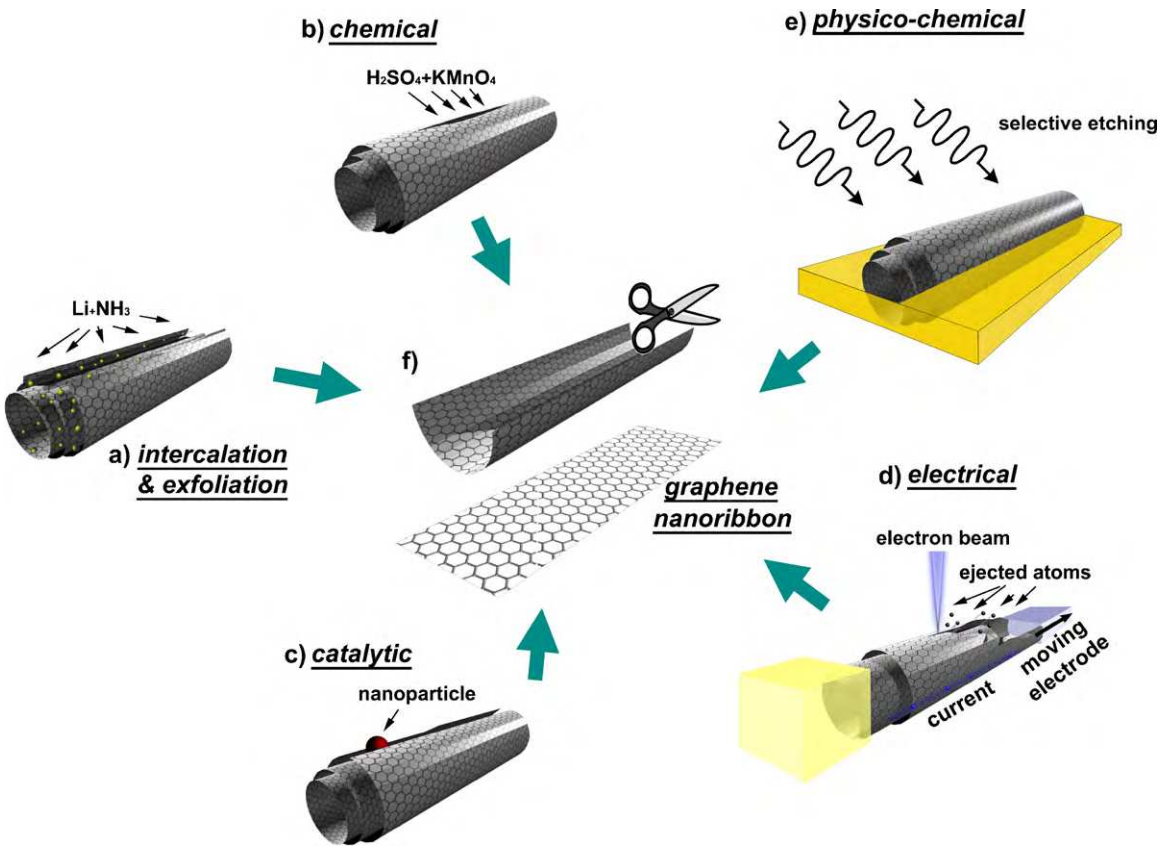

Figure 6 Sketch showing the different ways nanotubes could be unzipped to yield graphene nanoribbons (GNRs): (a) intercalation—exfoliation of MWCNTs, involving treatments in liquid NH_3 and Li, and subsequent exfoliation using HCl and heat treatments [104]; (b) chemical route, involving acid reactions that start to break carbon-carbon bonds (e.g. H_2SO_4 and $KMnO_4$ as oxidizing agents) [105]; (c) catalytic approach, in which metal nanoparticles ''cut'' the nanotube longitudinally like a pair of scissors [107,108], (d) the electrical method, by passing an electric current through a nanotube [109], and (e) physicochemical method by embedding the tubes in a polymer matrix followed by Ar plasma treatment [106]. The resulting structures are either GNRs or graphene sheets (f).

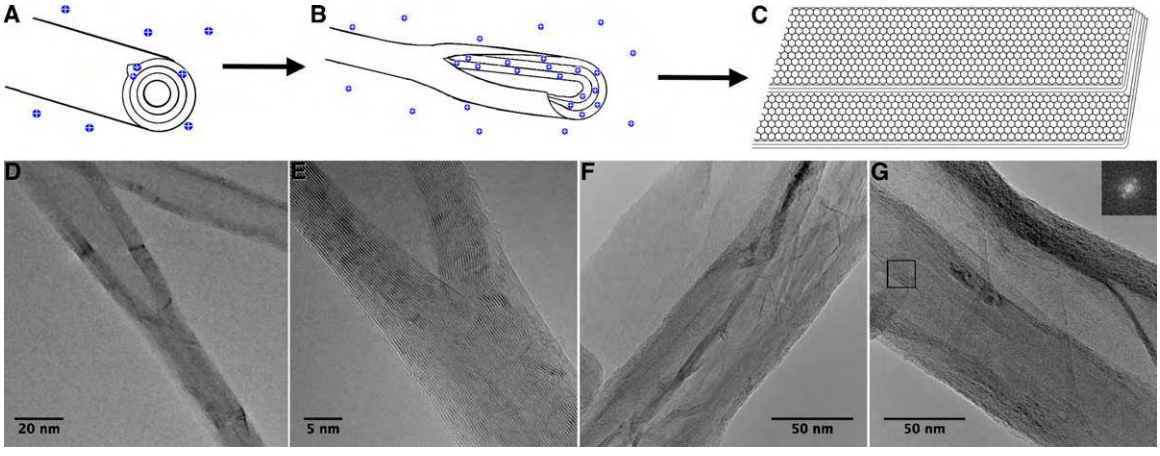

Figure 7 Schematics and representative images of the lithium-ammonia intercalation and exfoliation procedure to obtain nanoribbons from nanotubes. The process starts with cut MWCNT, open ends (and wall defects) allow intercalation of Li ions and NH_3 (a) in the negatively charged nanotubes. The intercalants push the walls to twice the interlayer distance of MWCNT initiating the fracture of nanotube walls (b). After acid and thermal treatments the exfoliation is complete and GNRs (''ex-MWCNT'') result (c). A HRTEM image (d) shows a partly opened GNR, a close up on the cleaved part (e) shows that after the process the graphitic layers can rearrange and recrystallize. The GNRs can comprise several layers of different thicknesses (f, g) The rearrangement to a graphitic order is confirmed by the hexagonal pattern of the Fast Fourier Transform (inset in g).

rial (''ex-MWCNTs'') contains up to 60% nanoribbons, with the rest partly opened (unzipped in parts) and damaged (sides and tips exfoliated but not unzipped) MWCNT, and graphene flakes peeled off the tube walls [104]. This mixture of products is partly due to the need to cut MWCNT to facilitate unzipping, as MWCNT longer than 2 μm rarely unzip fully lengthwise. Further improvements are needed to obtain full unzipping, and could lead to nanoribbons of relatively controlled dimensions dependent on the tubes that are unwrapped. The current mixture of by-products limits the applications of such materials (e.g. for electronic devices) unless separation and sorting methods could be devised. However, we should note that partially unzipped ex-MWCNTs could be of interest for composites (with the unwrapped edges interfacing to a matrix) and could also have interesting properties for nanoelectronics [110].

The group of James Tour [105] reported an oxidation method where MWCNTs are first opened due to permanganate oxidation, leading to unzipping nanotubes along their axis (Fig. 6b). The amount of oxidant used determines the degree of MWCNTs opening, but high efficiency and high yields (both nearing 100%) are reported. The nanoribbons obtained have oxidized edges, making them highly soluble in polar solvents. These ribbons can be reduced by hydrazine in order to remove the oxygen functional groups, thus restoring their good electrical conductivity. This method can also be applied to SWCNTs producing highly entangled and randomly stacked graphene sheets and ribbons. Although, it was believed that this route resulted in highly defective nanoribbons with relatively low electrical transport properties, Tour's group has now demonstrated that it is indeed possible to obtain highly crystalline graphene nanoribbons exhibiting extremely high electrical conductivities, which could be used in the fabrication of field effect transistors and other devices. The method involves an efficient chemical oxidation at 60 °C, in the presence of a second acid ($C_2HF_3O_2$ or H_3PO_4) besides the H_2SO_4—$KMnO_4$ mixture [111]. More recently and along this direction, Dai and coworkers have reported an alternative chemical method for unzipping carbon nanotubes by treating MWCNTs in air at 500 °C followed by the sonication of the resulting material in a DCE-PmPV solution [112]. These authors report that: (1) the ribbon material results in a high yield of unzipped tubes (e.g. 60%); (2) the edges of the unzipped tubes (or ribbons) appear to be smooth (although additional studies are needed in this direction); (3) the produced GNRs exhibit high conductance, low resistance and phase coherent transport and (4) the GNRs usually exhibit thicknesses of 2 or 3 layers.

The catalytic cutting method is attractive due to its simplicity (Fig. 6c), when compared to other chemical methods. Nevertheless, the actual amount of nanoribbons produced by this method (Fig. 8) is still very low (approximately 5% of the original CNT sample). Previous reports [113—115] have shown that the catalytic metal particle (Co or Ni) can cut graphene layers only along armchair or zigzag atomic lines (Fig. 8a). Metal nanoparticles are deposited on the surface of MWCNTs (via magnetron sputtering or chemically), and these coated tubes are subsequently placed on Si wafers and treated at 850 °C, under a low flow of H_2—Ar (Fig. 8a). The unzipping mechanism is based on the metal catalyst dissociating carbon bonds, and such carbon atoms reacting with H_2 to form methane (CH_4) [116] (see Fig. 8a). The samples revealed that the tubes were either cut, partially open, or open along the axis (Fig. 8b-e). Larger metal nanoparticles (ca. 40 nm) traveled along the axis of some carbon nanotubes, performing deeper cuts that opened longitudinally MWCNTs and N-doped MWCNTs (Fig. 8c and d) [108]. A similar route to unzip the tubes occurs by thermal treatment of nanotubes, encapsulating Fe nanoparticles, for 26 h at 1100 °C under an Ar atmosphere (Fig. 8e). It appears that at 1100 °C, the encapsulated Fe nanoparticles start to react with the surrounding carbon atoms, causing their dissociation and the breakage of the tube compartments. The nanoribbons produced in this way are typically 15—40 nm wide and 100—500 nm long. It is noteworthy that partially open MWCNTs have been predicted to exhibit a large magnetoresistance effect at low magnetic fields [110].

An alternative method consists in applying an electric current through a nanotube inside a microscope (Fig. 6d) [109]. Unfortunately, this method is only able to yield very low amount of unzipped nanotubes. However, experiments involving the passage of high currents through bulk nanotube samples should be tested and evaluated.

Another physicochemical method was also developed by Dai's group in 2009 [106]. MWCNTs are embedded in a poly(methyl metaacrylate) film, then turned over to expose the MWCNT walls which are etched away by an Ar plasma (Fig. 6e). The etching time determines whether single- or few-layered graphene nanoribbons are obtained. The method is much more laborious and yield is relatively low, *ca.* 20% with some MWCNT remaining, but these nanoribbons are more uniform in shape than those from other unzipping methods. It should be noted that partial opening of MWCNT by plasma etching had been reported as early as 2004 [117]. Here, the opened portions were compared to ''wings'', however the open ribbon-like segments were not longer than a few tens of a nanometer, and the process was neither controlled nor further developed.

The physical transformation of MWCNTs into nanoribbons is also possible, with the use of high pressure, though in many studies the target was to obtain diamond crystals. M. Zhang et al., reported that CVD grown MWCNTs annealed at high temperatures (950—1200 °C) under 5.5 GPa for 25 min, produce ribbon-like and onion-like graphitic structures [118], and higher temperatures favor ribbons (possibly collapsed nanotubes) over onions. Later on, the transformation of SWCNT bundles into nanoribbons has been reported [101] at high temperatures in vacuum. SWCNTs first coalesce into larger diameter SWCNTs or MWCNTs (from 1400 to 1600 °C). Such large diameter nanotubes collapse when the temperature is further increased at (*ca.* 1800 °C) in two types of GNRs, which can be differentiated by the shape of their closed ends.

Most of the methods mentioned above could produce very well defined and relatively crystalline nanoribbons, provided that the starting material is crystalline, uniform in length, diameter and number of layers. For some applications where edge uniformity is not necessary (e.g. composites), the production of kilogram amounts could be more relevant; two of the methods above appear easy to scale up. The catalytic cutting method is scalable, in principle, if large scale controlled deposition of nanoparticles over MWCNT can be achieved. The etching method does not seem amenable to scale up so easily as the others, but since it uses techniques

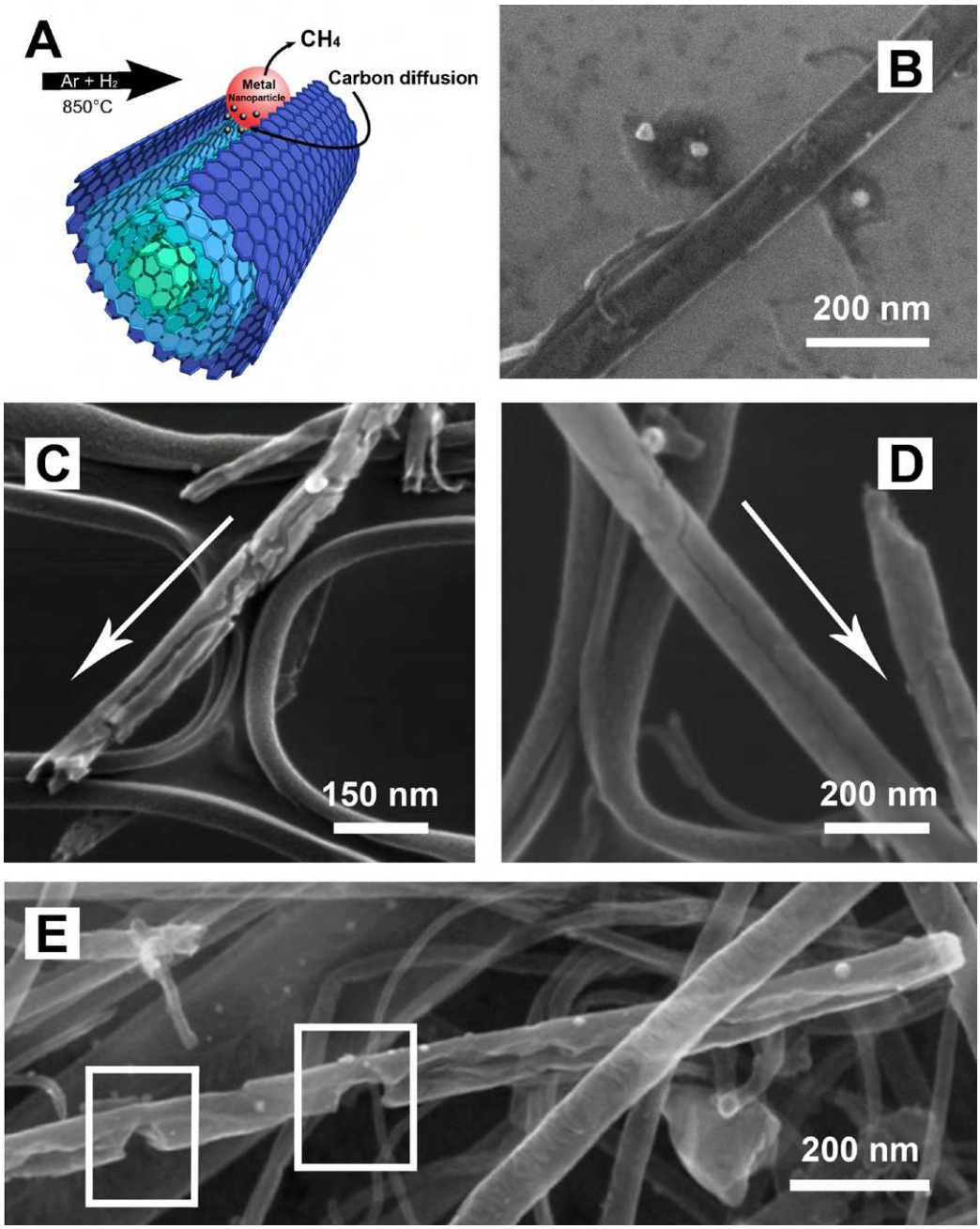

Figure 8 (a) Sketch depicting the carbon dissociation process occurring on the surface of metal nanoparticles (Co or Ni) at high temperature, and the subsequent formation of CH_4; (b) SEM micrograph of a graphitic nanoribbon as a result of the cutting experiments of MWCNTs with Co nanoparticles; (c) and (d) SEM images of N-doped MWCNTs, after hydrogenation of carbon performed with Ni sputtered catalyst nanoparticles [108], and (e) SEM image of an unzipped tube by the thermal treatment of nanotubes encapsulating Fe nanoparticles for 26 h at 1100 °C under an Ar atmosphere.

known in the semiconductor chip industry, it shows potential for integration in electronic devices. The chemical methods offer the possibility to control the lengths and widths of the resulting nanoribbons. However, challenges remain in controlling the nanotube opening processes, whether this occurs by exfoliation, etching, reduction or oxidation. In addition to challenges in controlling the opening of MWCNTs, a scalable process would have to provide conditions that prevent the agglomeration, wrinkling, and entanglement of the produced nanoribbons which are caused by van der Waals forces.

Other methods to produce graphene nanoribbons

Another widely used method to produce nanoribbons with very well defined crystallographic edges is by scanning tunneling lithography (STL). This technique consists on etching

carbon atoms using a scanning tunneling microscope (STM) tip relatively far from the sample. This approach takes advantage of a reaction involving the local decomposition of water molecules due to the electron flux between the tip and the sample under a negative bias. Upon the dissociation of water molecules, the carbon atoms at the surface react with oxygen to form carbon monoxide, and are etched away atom by atom [119]. Of course, such an atomic precision comes with a cost: unpractical production and a limited amount of ribbons using this method.

Micromechanical cleavage of graphene flakes has also been used to produce GNRs [120]. This technique uses a poly(dimethylsiloxane) (PDMS) stamp to remove graphite flakes off HOPG, and deposit them over an insulating surface. A second stamp then removes most of the graphite flakes and cleaves further the ones that remain on the surface. This produces a haphazard assortment of GNRs with widths ranging from 1 nm to a few μm and assorted lengths; most of them extending from a ''mother'' flake, and many of them with heights corresponding to a graphene monolayer. Although this does not seem a method for controlled and large scale production of GNRs, it provides a simple route to measure the electrical properties of assorted lengths and widths of GNRs. In this case the authors used conductance AFM for I-V measurements showing that the GNR behaved as semiconductors.

Electron irradiation at accelerating voltages >90 keV, is known to induce rearrangement of carbon atoms [121,122], which can lead to novel ordered structures. Such approach was used to locally transform electrospun poly(methyl methacrylate) (PMMA) nanofibers into graphene nanoribbons inside a HRTEM [123]. The graphene sheets align parallel to the e-beam, and once a nanoribbon is formed, further irradiation could reduce its thickness; suggesting the possibility of controlling the number of layers. The method however, does not produce crystalline arrangements at the junctions when crossed nanofibers are irradiated. These authors suggest that the same transformation might be possible with e-beam lithography, this however has not been proved and fine control over shape, size and edge structure of the graphene sheets appears to be difficult. [119,124,125].

Since most of these graphene nanoribbons could be homogenously dispersed in suspensions, different chemical reactions could be carried out and their use as drug deliverers, sensors and even composite fabrications could be tested and improved. All these potential applications are noteworthy besides the use of nanoribbons in nanoelectronic devices, as demonstrated above. In addition, these ribbon materials should now be tested in different toxicity assays.

Defects in graphene and graphitic nanoribbons

Defects play a crucial role in the properties of crystals and nanostructures, including graphitic systems. Graphene-like systems are so versatile that they can accommodate different kinds of defects that change completely their structure and also their physicochemical properties. In particular, defects which change the structure could also change the topology or the curvature. However, it is difficult to identify accurately and quantitatively the type of defects contained in graphene-like materials, and researchers have not been able to distinguish them systematically. Depending on the nature of the defective surface, the chemical activity of graphene may be quite different. For instance, the inclusion of twelve pentagons in a graphitic cluster can form a Fullerene and thus, the planar cluster becomes round with no boundaries. Such a spherical structure exhibits an electronegative surface which results in a very rich chemistry [4]. Similarly, the presence of heptagons and octagons could produce Schwarzite-like materials or nanotube networks with micropores where reactions can take place [33]. The inclusion of vacancies also alters the physicochemical properties of the graphitic systems producing ''antidot'' systems [126]. For graphitic nanoribbons, the most common defects are: vacancies, heptagon-pentagon pairs (Stone—Thrower—Wales type transformations, see below), loops and interstitials. While heptagon—pentagon pairs and loops preserve the connectivity of the nanoribbon, the interstitials and vacancies do not. Certainly, a challenge for the future will be the use of defects to design new graphitic nanoribbons with specificity for sensing different kinds of molecules or to anchor specific polymer chains in order to produce stable and well dispersed composites.

In general, defects within graphene-like structures could be categorized in five different groups (Fig. 9):

(1) *Structural defects*, related to imperfections that significantly distort the curvature of the hexagonal carbon lattice. These defects are usually caused by the presence of non-hexagonal rings (e.g. pentagons, heptagons, or octagons) surrounded by hexagonal rings. For example if a single or a few pentagons are embedded into the graphene lattice, nanocones with different apex angles are obtained (Fig. 9a). A 30° angle in a SWCNT, could also be explained by the presence of pentagon on one side of the tube and a heptagon on the opposite side. The reactivity of pentagons, heptagons or octagons with specific acceptor or donor molecules has still to be determined from the theoretical and experimental stand points.
(2) *Bond rotations or grain boundaries*, occurring on graphene surfaces, which do not result in large curvature distortions of the sheet (Fig. 9b). In particular, these defects could be 5-7-7-5 pairs embedded in the hexagonal network or Stone—Thrower—Wales (STW-type) defects [127,128] that could be created by rotating a carbon—carbon bond 90° within four neighbouring hexagons, thus resulting in the transformation of two pentagons and two heptagons [129,130]. 2D planar graphene-like systems containing pentagons, hexagons and heptagons, called Haeckelites, have been proposed and found to be metallic in theoretical studies [23]. Nanoribbons constructed from Haeckelites could be considered as new hypothetical nano-architectures with fascinating properties that could be applied in electronics. Isolated pentagon-heptagon pairs could also be introduced to form a grain boundary in graphene [128] or in a graphitic nanoribbon, thus changing their edge termination and electronic properties, forming a hybrid graphitic nanoribbon (Fig. 10). These particular hybrid nanoribbons exhibit half metallicity in the absence of an electric field (Fig. 10b), and could be used to transport electrons with one type of spin; which could be a step forward in new spintronic devices [131]. It is note-

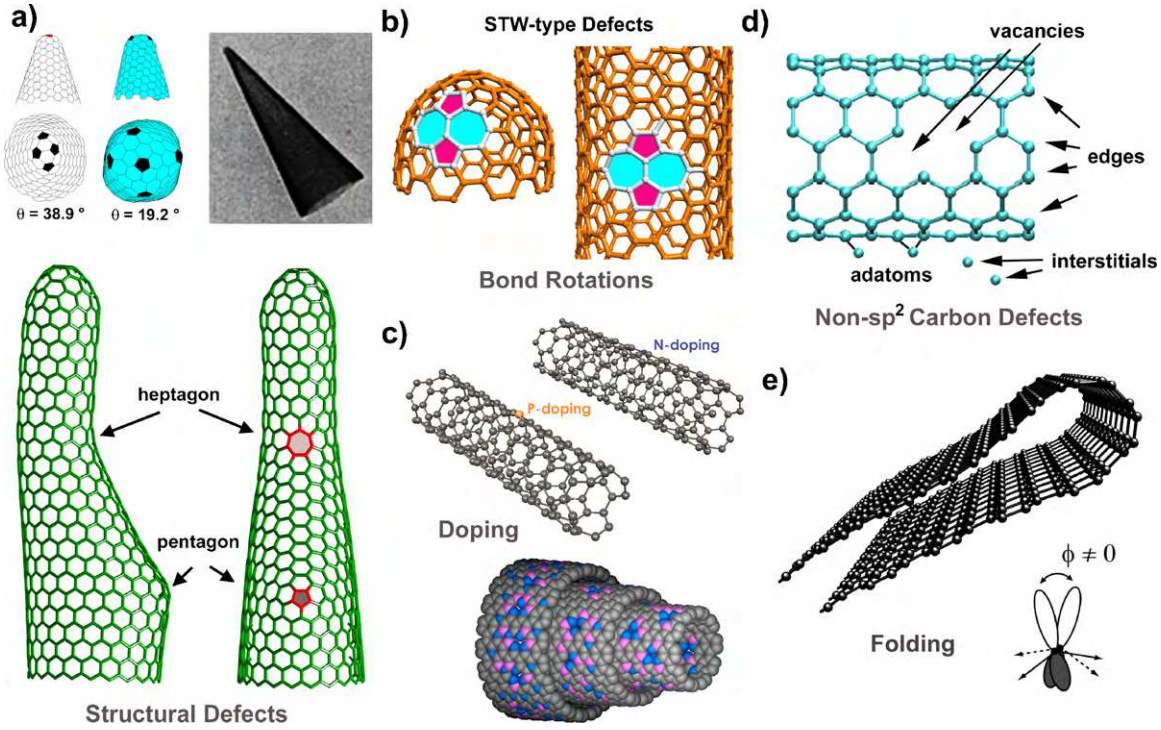

Figure 9 Schematic models representing different types of defects in graphene-like materials. (a) *Structural defects* induce significant structural changes caused by the presence of pentagons or heptagons within the hexagonal sp^2 hybridized carbon lattice (Image of cones courtesy of M. Endo and T.W. Ebbesen); (b) *Topological defects*, also termed Stone-Thrower-Wales defects, do not result in big structural changes. Shown here is the formation of 5-7-7-5 pairs created by rotating an individual carbon-carbon bond 90°; (c) *Doping* consists of replacing a carbon atom with another element within the hexagonal lattice (here, N and P) or a CNT randomly doped with B and N; (d) *Non-sp^2 hybridized carbon defects*, including vacancies, edges, adatoms, interstitials, carbon chains, etc.; (e) *Folding-induced defects*, which result from significant deformation of the graphene sheet, thus altering the π orbitals. The direction of the π orbital is then called the π orbital axis vector (POAV). The angle $\theta_{\sigma\pi}$ between the POAV and a σ direction (i.e., a bond) indicates the degree of ''pyramidalization'' and the hybridization. For $\theta_{\sigma\pi} = 90^\circ$ (planar system), the σ orbitals are in a sp^2 hybridization and the π orbital is a pure p_z orbital. For a folded graphene sheet, $\theta_{\sigma\pi}$ has an intermediate value which decreases as the inverse of the radius of the curvature of the folding, and reaches 90° at the limit $R \rightarrow \infty$.

worthy that the electronic and chemical properties of these 5-7 or 5-7-7-5 pairs (Fig. 10c) are different from the structural defects (see above) and their reactivity and detection needs to be investigated theoretically and experimentally. Recently, Zettl and coworkers were able to observe directly 5-7 and STW defects on isolated graphene surfaces using aberration corrected transmission electron microscopy (Fig. 10d, also see movies from supplementary material of [65]).

(3) *Doping-induced defects*, arising from substitutional non-carbon atoms embedded in the graphitic lattice (Fig. 9c). In this case, it has been demonstrated that nitrogen and boron atoms can be introduced into the hexagonal sp^2 hybridized carbon lattice. With both dopants, the chemical reactivity of the graphene surface increases, in one case due to the fact that N has one electron more than C, in the other because B has one electron less than C. Therefore, these type of defects could be used to tune the type of conduction in graphene-like materials, ranging from n-type transport (substitutional nitrogen doping) to p-type conduction (substitutional boron atoms in the lattice) [132]. Recent studies have demonstrated that other elements such as P, S, Si and paired dopants such as P-N could also be introduced in the hexagonal lattice of carbon tubules [133—135,38,136]. Therefore, the insertion of non-carbon atoms in graphene-like materials could tailor the chemical reactivity and electronic transport of the layers and further work along this research line needs to be carried out [136].

(4) *Non-sp^2 carbon defects* caused by the presence of highly reactive carbons such as dangling bonds, carbon chains, interstitials (free atoms trapped between SWCNTs or between graphene sheets), edges (open nanotubes), adatoms and vacancies (Fig. 9d). These defects are usually observed in a HRTEM, when the adsorbed atoms on these reactive sites are removed by the electron beam energy. It has been demonstrated that the creation of such defects could promote the formation of covalent nanotube junctions [137] and trigger the coalescence of nanotubes [138]. However, for nanoribbons, the dynamics of these defects has not been investigated and further research is required in this direction.

(5) *High-strain folding of graphene sheets* (loop formation), which can be induced by annealing two adjacent graphene layers (Fig. 9e). These types of ''loops'' have often been observed in thermal annealing occurring at above 1500 °C [42,86,87,139], but their chemical

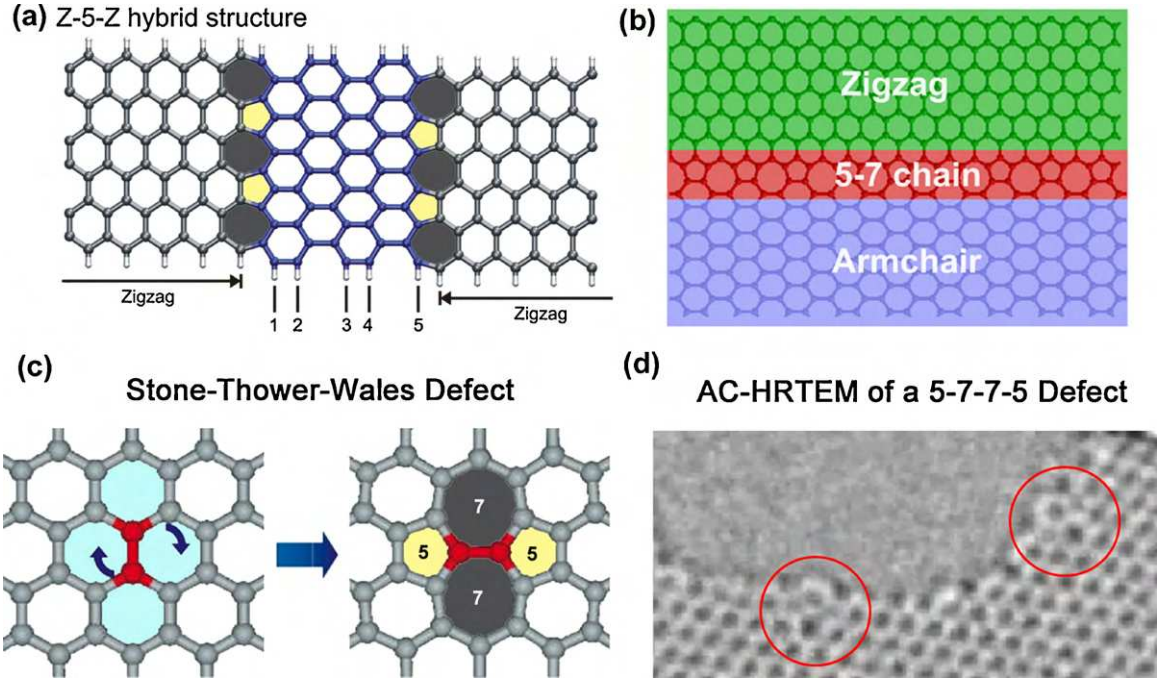

Figure 10 (a) Molecular model of a hybrid structure with zigzag leads connected by 5-7 chains to an armchair segment with $N_A = 5$ (Z-5-Z hybrid structure); (b) Molecular model of ordered arrays of pentagon-heptagon defects on a hybrid-graphene nanoribbon [131]; (c) Molecular model showing the transformation of 4 adjacent hexagons into a 5-7-7-5 defect or Stone-Thrower-Wales defect, and (d) HRTEM images showing two 5-7-7-5 defects located on the edges (red circles) of a hole in a graphene surface (images taken from movies from supplementary material of Ref. [65]).

reactivity and electronic properties have not been investigated in detail. In fullerene (or carbon cage) chemistry, the main type of defect is *structural*, which deals with the presence of pentagonal rings that induce a highly curved and reactive molecule caused by the mixture of π and σ orbitals. In nanotube chemistry, these structural defects mainly occur on the caps (where pentagons are located). Narrow or highly curved nanotubes (usually <1 nm diameter) would also be more reactive. In highly crystalline SWCNT samples, the caps are a small portion of the structure and other highly curved areas are not present since the nanotubes usually have diameters larger than 1 nm. Therefore, graphene and nanotube chemistry require a better understanding of the defects mentioned above, in order to induce and control strong (or weaker) covalent (or $\pi-\pi$) interactions with other molecules, atoms, or clusters.

It should be noted that buckling and folding can be induced deliberately in graphene. Bao et al. have reported controlled rippling of suspended graphene sheets [140]. Li et al. [141] have also reported deliberate formation of ripples in graphene flakes deposited over polymethylmetacrylate (PMMA), by heating above the glass transition temperature of PMMA, upon rapid cooling the polymer shrinks more than the graphene, and the stresses lead to periodic sinusoidal (lambda = 550 nm) buckles in the edges of graphene sheets. Raman spectroscopy shows a blue shift consistent with a compressive stress on the graphene sheet. The authors also report that this process can lead to folding of graphene flakes into few-layer graphene but this does not seem to be a controlled process. Other processing approaches are likely to appear in the literature extending the possibility of controlling folding and buckling of GNRs.

Doped graphitic nanoribbons

Doping of graphene and graphene nanoribbons is relevant because, depending on the location of the dopants and their concentration, their physicochemical properties could be tuned and controlled. In this context, Cervantes-Sodi, et al. [142] reported theoretical studies related to the doping of graphene nanoribbons with N, B and O atoms. They noted that when doping nanoribbons, edge-type and substitutional doping induce different electronic properties to the systems and, in some cases, half-metallic behavior. The band gap could be tuned by doping and when zigzag ribbons possessed substitutional nitrogen at 1.7 at%, the ribbons were metallic. Similar studies have reported the effects of N doping in zigzag nanoribbons [143]. Roche and coworkers predicted the electronic transport of nanoribbons with different concentration of dopants, and observed that different materials exhibiting different band gaps could be obtained [144]. Therefore, the doped-graphene nanoribbons appear to be excellent candidates in the design of novel electronic devices and transistors and further theoretical and experimental work are needed; the study of their chemical activity also needs to be carried out.

Experimentally, a N-doped-graphene-like structure has been realized using a CVD process which generated both edge-type and substitutional N doping [145]. These authors

found that the doped-graphene-like material exhibited an n-type semiconducting behavior, and contained between 2 and 6 layers with a variable N concentration (i.e., 1.2—8.9 at%), depending on the NH_3 flow rate used in the CVD process. Subsequently, Dai's group successfully produced graphene nanoribbons doped with nitrogen *via* joule heating in the presence of NH_3 [146]. The process produced edge-type and substitutional nitrogen doping, and $-NH_2$ groups attached to the ribbon edges. They also found theoretically that the presence of C=O bonds on edges resulted on p-doped GNRs. Finally, N-doped graphic nanoribbons have been produced by unzipping CN_xMWNTs via their catalytic hydrogenation [108].

Although the literature regarding doped-graphene nanoribbons is very scarce, it is clear that doping appears to be a reliable way to control the electronic and chemical properties of the ribbons, and further work should focus on this direction. In this context, doping experiments with B, P and Si could also lead to novel graphene-like materials and novel unzipping methods of already available doped-carbon nanotubes (e.g. C_xB_y-MWNTs, C_xSi_y-MWNTs, $C_xP_yN_z$-MWNTs, etc.) should be explored.

Characterization of graphene materials by Raman spectroscopy and other techniques

In the early days of the study of graphene, with the use of the optical microscope, the identification of graphene flakes was a simple but tedious task. Quantifying the number of layers implied the use of time consuming techniques (AFM, TEM) and required prior sample preparation. However, in 2006, Ferrari et al. reported the Raman spectra of single-, double- and few-layer graphene produced with Novoselov's ''scotch-tape'' technique [147]. Clear signals specific for each single-, double and few (<5) layer graphene were identified. Therefore, Raman spectroscopy has become a very useful technique for the characterization of graphene and GNRs.

Raman spectroscopy stands as a powerful characterization technique of all types of carbon nanostructures. The most prominent features in the Raman spectra of sp^2 hybridized carbon materials are the G-band appearing at *ca.*1580 cm^{-1} and the G′-band at *ca.* 2700 cm^{-1} for a laser excitation energy of 2.41 eV. When carbon materials have a certain amount of disorder or edges within the structure, a disorder-induced band appears, the so-called D-band, at *ca.*1350 cm^{-1}. The G-band is associated with the doubly degenerate (iTO and LO) phonon mode (E_{2g} symmetry) at the Brillouin zone center. On the other hand, the G′- and the D-bands originate from second-order processes, involving two iTO phonons near the K point for the G′-band or one iTO phonon and one defect for the D-band [148].

In Ferrari's report, the G′-band was shown to have a different peak shape for single-, double- and few-layer graphene; it is worth mentioning that the studied graphene flakes were exfoliated from highly oriented pyrolytic graphite (HOPG), having thus a well achieved AB Bernal stacking [147]. The G′-band of single-layer graphene, measured with a laser energy of 2.41 eV, exhibits a single excitation at 2700 cm^{-1} with a FWHM of 24 cm^{-1}. In addition, the relative intensity of the G′-band is larger than that of the G-band. The G′-band of double-layer graphene exhibits four excitations, whereas the spectra of five layers and more are hardly distinguishable from that of bulk graphite. Subsequent works allowed the identification of the number of layers (1, 2, 3 and 4) by Raman spectroscopy using the G′-band. For turbostratic or misoriented double or few-layer graphene, where the stacking of the graphene sheets is rotationally random with respect to one another along the *c* axis, the Raman G′ band appears as a single Lorentzian, very similar to that of single-layer graphene but with a larger line width [26,148,149]. Thus, when a graphene sample is produced with other methods than the micromechanical exfoliation of HOPG and the interlayer interaction is absent or not very strong, the G′ Raman band cannot be used as a direct identification tool to quantify the number of layers.

It is noteworthy that imperfections in the graphene lattice such as dopants could introduce new features in the G′-band. In this context, the presence of a defect-induced feature (G'_{Def} band) in the immediate-vicinity of the second-order G'_{Pris} band (located at ~2600—2700 cm^{-1} for E_{laser} = 2.41 eV or λ = 514 nm) has provided valuable information about charged defects present in single-walled carbon nanotubes (Fig. 11) [136]. In addition, it has been demonstrated that for doped nanotubes, the relative intensity of the G'_{Def} is proportional to the amount of dopants in the tube material. Similarly, the effect of doping graphitic systems either electrochemically or by an electric field can be observed by Raman spectroscopy. Due to renormalization of the phonon energies and the resultant change on the effective force constants of atomic vibrations, there is an increase of the frequency and a decrease of the line width of the G-band in monolayer graphene [150]. For the case of bilayer graphene, a split of the G-band occurs at negative gate voltages [151]. All these observations demonstrate that Raman spectroscopy could be very useful in determining the type of doping in nanoribbons but extensive work needs to be done in this direction.

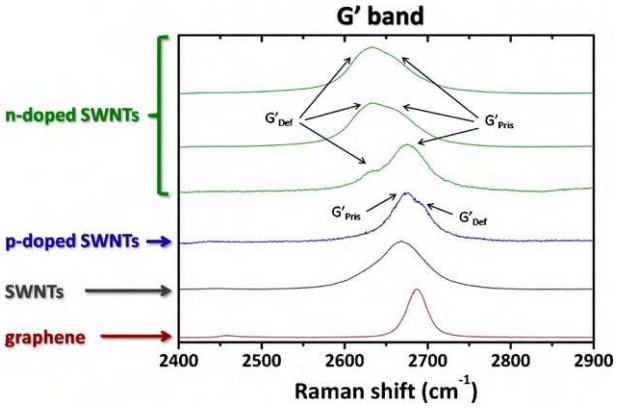

Figure 11 The G′-band Raman band of different sp^2 hybridized carbon materials (nanotubes) measured at room temperature with E_{laser} = 2.41 eV (514 nm). The arrows point to defect-induced peaks in the G′ for doped SWCNTs (G'_{Def}). The p/n doping signal arises from substitutional boron or nitrogen atoms, the nearest neighbours of carbon in the periodic table. The spectra of graphene and SWCNTs (G'_{Pris}) is shown for comparison (data provided by I.O. Maciel) [136].

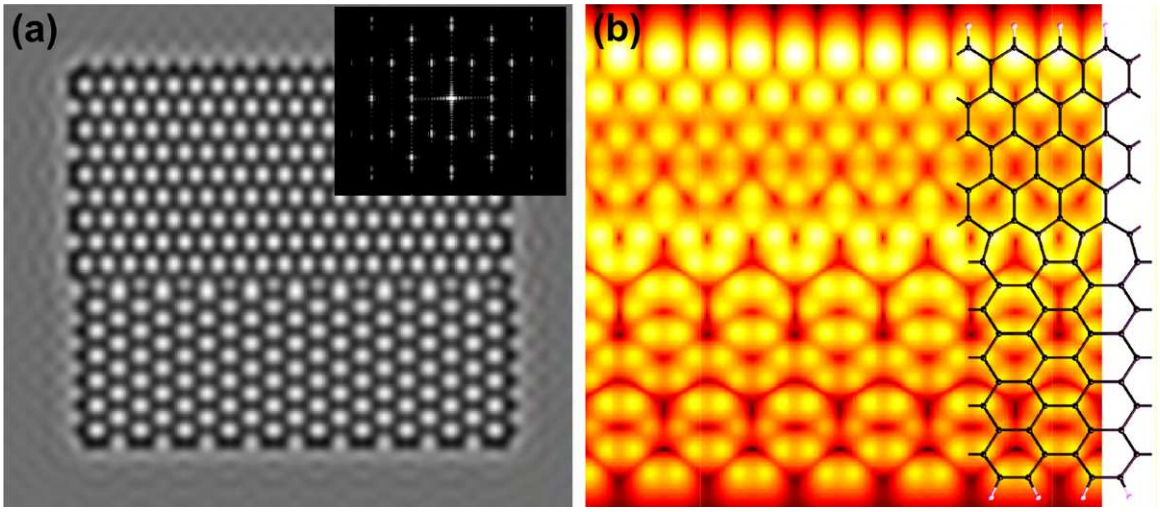

Figure 12 (a) Simulated high-resolution electron microscopy image of a graphene-like nanostructure with a grain boundary formed by pentagons and heptagons where the edges of the sheet change from armchair to zigzag. The inset shows a simulated diffraction pattern showing twelve spots characteristic of armchair and zigzag features in the same structure. (b) Simulated STM image of the same system illustrating a lack of one to one correspondence between the image and the structure.

Under the right conditions, electron diffraction could be used to obtain information from graphene-like structures. In addition, it is possible to simulate images and electron diffraction patterns using the coordinates of the nanostructure (for example with SimulaTem [152]), and then compare them with the experimental diffraction patterns and high-resolution images. In Fig. 12a a simulated HRTEM image and its corresponding diffraction pattern of a graphene piece with a grain boundary formed by 5—7 defects is shown. It is therefore clear that defects on graphene surfaces could be identified by electron diffraction.

Scanning tunneling microscopy (STM) and spectroscopy (STS) could be powerful tools to identify and obtain electronic information about defects in graphene surfaces and nanoribbons. These characterization techniques can give very valuable information on both the structure of the graphene or GNR surface, and on its electronic structure close to the Fermi level. However, the interpretation of such images can be difficult, and thus simulation of such images is often very helpful (Fig. 12b). Very recently, Batzill and coworkers identified the presence of a 5-8-5 defect line within a graphene sheet using STM [153]. In particular, these authors noted that this defect line was able to behave as a quantum wire. Additionally, as discussed in Section 5, it is conceivable to construct defective graphene-like sheets with other types of defects similar to Haeckelites. Therefore, additional theoretical and experimental studies regarding defects in graphene are urgently needed to develop further graphene-based electronics.

Applications

Graphene is a unique material because its displays an outstanding electron transport at room temperature, in which electrons behave as massless particles without experiencing scattering. Therefore, the imminent applications of this layered material are in electronics such as in the fabrication of ultrafast transistors [154] able to operate in the terahertz frequency range. Its low capacitance is also important in the fabrication of biosensors or chemical sensors due to the resulting low values of the signal to noise ratios. However, due to the large number of reactive edges in graphene nanoribbons, it is expected that the sensing abilities of ribbons are superior to those shown in graphene. In addition, by doping or by applying different edge spin orientations, the bandgap of nanoribbons may be controllable, thus having important implications in the fabrication of novel and ultrafast electronic nanodevices with outstanding sensing abilities. Research in this direction needs to be addressed from the experimental and theoretical standpoints but there are already some promising results. Lin et al. [155] have shown that wafer scale production of graphene (grown epitaxially over SiC) FETs is possible and such circuits have 100 GHz switching frequencies.

In addition to transistors, GNRs could find applications in nano-electromechanical systems (NEMS). An example of this was reported by Wei et al. [94] who produced a few-layer graphene ribbon NEM switch with good reversibility, which was used in an OR gate.

From the materials science point of view, graphene and graphene nanoribbons could be used as fillers in the fabrication of robust polymer composites, highly conducting transparent films, high thermal conducting polymers, and other composites with different metals and ceramics. Due to the presence of defects and dopants, it may also be possible to use these locations as catalytic spots for anchoring specific bio-molecules, drugs, heavy metals, and other species.

Another application for graphene is as the thinnest possible support film for HRTEM, this has been shown to allow, for example, observation of individual adatoms over graphene [156] and atomic resolution imaging of soft hard interfaces [157]. These graphene film grids can easily be made in the laboratory by transferring graphene flakes over TEM grids, and are starting to be commercially available. Few-layer graphene films have also been shown to offer advantages in TEM.

There are numerous challenges still to be achieved. In this respect, the bulk production (e.g. tons per year) of graphene and graphitic nanoribbons may be achieved by unzipping carbon nanotubes but further experiments need to be performed. It is clear that graphene nanoribbons could now be dispersed in suspensions due to the reactivity of the large number of edges sites. Therefore, edge chemistry and physics of the ribbons, a field which is just arising, should now lead to: (a) novel catalytic reactions, (b) sensor fabrication, (c) the production of field effect transistors, (d) the generation of electrodes for Li-ion batteries, (e) the assembly of heavy metal filters, (f) the fabrication of highly conducting, transparent polymer composites and other composites with metals and ceramics, g) drug deliverers, etc. However, controlled defect engineering is needed in order to fine tune the chemical, electronic, mechanical, magnetic and thermal properties of graphitic nanoribbons.

Porous graphene or chemically activated graphene with ''holes'', also referred in the literature as antidots [126,158,159] should be studied in detail from the experimental and theoretical standpoints. It is possible that this ''holey'' material could be applied in catalysis, heavy metal adsorption, sensors and other uses. Porous graphene with controlled passivation of the dangling bonds in the pores has been predicted to be a very selective membrane for gas separation [160]. In this context, theoretical research should also target the use of GNRs as constructing building blocks to generate more complicated 2D and 3D networks (Fig. 1p), which will certainly result in novel porous materials with unprecedented mechanical, chemical, magnetic and electronic properties.

Conclusions

The production of GNRs is a rapidly advancing field, and novel synthetic methods and advances towards their applications will be developed. A challenge however will remain for facile integration of graphene into electronic devices: control over the deposition of GNRs, control on the atomic edge arrangements and creating efficient electrical contacts. This is only the tip of the iceberg since other layered materials such as BN, MoS_2, WS_2, ZnO, TiO_2, etc., could also generate nanoribbons. In this context, it has been demonstrated that BN nanoribbons exhibiting zigzag edges could behave as metal and even emit electrons and low turn on voltages [161]. Very recently the group of Ajayan reported the synthesis of a monolayer hybrid BNC material that exhibits hexagonal structure. The electrical properties of such hybrid BNC films range from insulating to conducting, and could be controlled by varying the C concentration within the sample [162]. Other ribbons such as ZnO [163,164] or MoS_2 [165] could be metallic and even exhibit ferromagnetic properties. Therefore, the possibilities to construct other types of devices using different types of nanoribbons, and the conception of hybrid ribbons may be the way to develop layered electronics and materials science. It is clear that theorists and experimentalists should join efforts in order to tackle these complicated problems, especially those related to applications.

We believe that the general principles and concepts laid out in this account should be useful to readers starting working on graphene and graphene nanoribbons. Regarding their characterization, microscopy (SPM and electronic) together with micro-Raman spectroscopy will be key tools to identify and understand the basics of defects in graphene-like systems. The controlled use of defects for tailoring the physicochemical of graphene and GNRs properties should be exploited further, similar to doping for the silicon industry. In addition, the extreme sensitivity of GNRs to small variations in, for instance edge chemistry or stacking order, can be advantageous for some applications (e.g. sensing, switching, data storage, drug delivery, etc.), and could also be used to control the performance of different devices. As in many other discoveries in nanoscience, theoretical and experimental approaches should occur synergistically in order to advance the field even more rapidly.

References

[1] H.W. Kroto, J.R. Heath, S.C. O'Brien, R.F. Curl, R.E. Smalley, Nature 318 (1985) 162.
[2] M.S. Dresselhaus, G. Dresselhaus, P.C. Eklund, Science of Fullerenes and Carbon Nanotubes: Their Properties and Applications, Academic Press, 1996.
[3] K.M. Kadish, R.S. Ruoff, Fullerenes, Wiley-IEEE, 2000.
[4] A. Hirsch, M. Brettreich, Fullerenes, Wiley-VCH, 2005.
[5] H.W. Kroto, K. McKay, Nature 331 (1988) 328.
[6] D. Ugarte, Nature 359 (1992) 707.
[7] A. Chuvilin, U. Kaiser, E. Bichoutskaia, N.A. Besley, A.N. Khlobystov, Nat Chem (2010), advance online publication.
[8] A. Oberlin, M. Endo, T. Koyama, J. Cryst. Growth 32 (1976) 335.
[9] S. Iijima, Nature 354 (1991) 56.
[10] P. Ball, Nature 354 (1991) 18.
[11] S. Iijima, T. Ichihashi, Nature 363 (1993) 603.
[12] D.S. Bethune, C.H. Klang, M.S. de Vries, G. Gorman, R. Savoy, J. Vazquez, R. Beyers, Nature 363 (1993) 605.
[13] A. Krishnan, E. Dujardin, M.M.J. Treacy, J. Hugdahl, S. Lynum, T.W. Ebbesen, Nature 388 (1997) 451.
[14] B.W. Smith, M. Monthioux, D.E. Luzzi, Nature 396 (1998) 323.
[15] S. Iijima, M. Yudasaka, R. Yamada, S. Bandow, K. Suenaga, F. Kokai, K. Takahashi, Chem. Phys. Lett. 309 (1999) 165.
[16] J. Liu, H. Dai, J.H. Hafner, D.T. Colbert, R.E. Smalley, S.J. Tans, C. Dekker, Nature 385 (1997) 780.
[17] K.S. Novoselov, A.K. Geim, S.V. Morozov, D. Jiang, Y. Zhang, S.V. Dubonos, I.V. Grigorieva, A.A. Firsov, Science 306 (2004) 666.
[18] H.P. Boehm, A. Clauss, G.O. Fischer, U. Hofmann, Zeitschrift Für Anorganische Und Allgemeine Chemie 316 (1962) 119.
[19] Y. Gan, W. Chu, L. Qiao, Surf. Sci. 539 (2003) 120.
[20] A.K. Geim, K.S. Novoselov, Nat. Mater. 6 (2007) 183.
[21] A.H. Castro Neto, F. Guinea, N.M.R. Peres, K.S. Novoselov, A.K. Geim, Rev. Mod. Phys. 81 (2009) 109.
[22] V.H. Crespi, L.X. Benedict, M.L. Cohen, S.G. Louie, Phys. Rev. B 53 (1996) R13303.
[23] H. Terrones, M. Terrones, E. Hernández, N. Grobert, J.C. Charlier, P.M. Ajayan, Phys. Rev. Lett. 84 (2000) 1716.
[24] A.M. Affoune, B.L.V. Prasad, H. Sato, T. Enoki, Y. Kaburagi, Y. Hishiyama, Chem. Phys. Lett. 348 (2001) 17.
[25] C. Berger, Z. Song, X. Li, X. Wu, N. Brown, C. Naud, D. Mayou, T. Li, J. Hass, A.N. Marchenkov, E.H. Conrad, P.N. First, W.A. de Heer, Science 312 (2006) 11916.
[26] A. Reina, X. Jia, J. Ho, D. Nezich, H. Son, V. Bulovic, M.S. Dresselhaus, J. Kong, Nano Lett. 9 (2009) 30.
[27] K.S. Kim, Y. Zhao, H. Jang, S.Y. Lee, J.M. Kim, K.S. Kim, J. Ahn, P. Kim, J. Choi, B.H. Hong, Nature 457 (2009) 706.

[28] C. Fantini, E. Cruz, A. Jorio, M. Terrones, H. Terrones, G. Van Lier, J.C. Charlier, M.S. Dresselhaus, R. Saito, Y.A. Kim, T. Hayashi, H. Muramatsu, M. Endo, M.A. Pimenta, Phys. Rev. B 73 (2006) 193408.
[29] M. Endo, Y. Kim, T. Hayashi, H. Muramatsu, M. Terrones, R. Saito, F. Villalpando-Paez, S. Chou, M.S. Dresselhaus, Small 2 (2006) 10316.
[30] H. Terrones, M. Terrones, New J. Phys. 5 (2003) 1266.
[31] A.A. Zakhidov, R.H. Baughman, Z. Iqbal, C. Cui, I. Khayrullin, S.O. Dantas, J. Marti, V.G. Ralchenko, Science 282 (1998) 897.
[32] T. Kyotani, Carbon 38 (2000) 269.
[33] P. Kowalczyk, R. Holyst, M. Terrones, H. Terrones, Phys. Chem. Chem. Phys. 9 (2007) 17862.
[34] E. Terrés, B. Panella, T. Hayashi, Y. Kim, M. Endo, J. Dominguez, M. Hirscher, H. Terrones, M. Terrones, Chem. Phys. Lett. 403 (2005) 363.
[35] J.M. Romo-Herrera, M. Terrones, H. Terrones, S. Dag, V. Meunier, Nano Lett. 7 (2007) 570.
[36] J.M. Romo-Herrera, M. Terrones, H. Terrones, V. Meunier, Nanotechnology 19 (2008) 315704.
[37] X. Lepró, Y. Vega-Cantú, F. Rodríguez-Macías, Y. Bando, D. Golberg, M. Terrones, Nano Lett. 7 (2007) 22206.
[38] J.M. Romo-Herrera, D.A. Cullen, E. Cruz-Silva, D. Ramírez, B.G. Sumpter, V. Meunier, H. Terrones, D.J. Smith, M. Terrones, Adv. Funct. Mater. 19 (2009) 11939.
[39] R. Saito, G. Dresselhaus, M.S. Dresselhaus, Physical Properties of Carbon Nanotubes, Imperial College Press, 1998.
[40] K.S. Novoselov, A.K. Geim, S.V. Morozov, D. Jiang, M.I. Katsnelson, I.V. Grigorieva, S.V. Dubonos, A.A. Firsov, Nature 438 (2005) 197.
[41] Y. Zhang, Y. Tan, H.L. Stormer, P. Kim, Nature 438 (2005) 201.
[42] Z. Liu, K. Suenaga, P.J.F. Harris, S. Iijima, Phys. Rev. Lett. 102 (2009) 015501.
[43] Y. Zhang, T. Tang, C. Girit, Z. Hao, M.C. Martin, A. Zettl, M.F. Crommie, Y.R. Shen, F. Wang, Nature 459 (2009) 820.
[44] B. Partoens, F.M. Peeters, Phys. Rev. B 75 (2007) 193402.
[45] B. Partoens, F.M. Peeters, Phys. Rev. B 74 (2006) 075404.
[46] S.V. Morozov, K.S. Novoselov, F. Schedin, D. Jiang, A.A. Firsov, A.K. Geim, Phys. Rev. B 72 (2005) 201401.
[47] I.A. Luk'yanchuk, Y. Kopelevich, Phys. Rev. Lett. 97 (2006) 256801.
[48] S. Latil, V. Meunier, L. Henrard, Phys. Rev. B 76 (2007) 201402.
[49] A.A. Balandin, S. Ghosh, W. Bao, I. Calizo, D. Teweldebrhan, F. Miao, C.N. Lau, Nano Lett. 8 (2008) 902.
[50] W. Cai, A.L. Moore, Y. Zhu, X. Li, S. Chen, L. Shi, R.S. Ruoff, Nano Lett. 10 (2010) 16451.
[51] C. Lee, X. Wei, J.W. Kysar, J. Hone, Science 321 (2008) 385.
[52] I.W. Frank, D.M. Tanenbaum, A.M. van der Zande, P.L. McEuen, AVS, 2007, pp. 2558–2561.
[53] V.M. Pereira, A.H. Castro Neto, N.M.R. Peres, Phys. Rev. B 80 (2009) 045401.
[54] M. Farjam, H. Rafii-Tabar, Phys. Rev. B 80 (2009) 167401.
[55] R.M. Ribeiro, V.M. Pereira, N.M.R. Peres, P.R. Briddon, A.H. Castro Neto, New J. Phys. 11 (2009) 115002.
[56] S.B. Bon, L. Valentini, R. Verdejo, J.L. Garcia Fierro, L. Peponi, M.A. Lopez-Manchado, J.M. Kenny, Chem. Mater. 21 (2009) 34338.
[57] S. Osuna, M. Torrent-Sucarrat, M. Sola; P. Geerlings, C.P. Ewels, G.V. Lier, J. Phys. Chem. C 114 (2010) 33405.
[58] B. Wang, B.J. Cooley, S.-. Cheng, K. Zou, Q.Z. Hao, F. Okino, J. Sofo, N. Samarth, J. Zhu, APS March Meeting 2010 Abstracts, American Physical Society, 2010.
[59] J.O. Sofo, A.S. Chaudhari, G.D. Barber, Phys. Rev. B 75 (2007) 153401.
[60] A.K. Geim, K.S. Novoselov, D.C. Elias, R.R. Nair, T.M.G. Mohiuddin, S.V. Morozov, P. Blake, M.P. Halsall, A.C. Ferrari, D.W. Boukhvalov, M.I. Katsnelson, Science 323 (2009) 610.
[61] P. Sessi, J.R. Guest, M. Bode, N.P. Guisinger, Nano Lett. 9 (2009) 43437.
[62] D.A. Dikin, S. Stankovich, E.J. Zimney, R.D. Piner, G.H.B. Dommett, G. Evmenenko, S.T. Nguyen, R.S. Ruoff, Nature 448 (2007) 457.
[63] S. Park, R.S. Ruoff, Nat. Nano 4 (2009) 217.
[64] X. Jia, M. Hofmann, V. Meunier, B.G. Sumpter, J. Campos-Delgado, J.M. Romo-Herrera, H. Son, Y. Hsieh, A. Reina, J. Kong, M. Terrones, M.S. Dresselhaus, Science 323 (2009) 17015.
[65] S.G. Louie, A. Zettl, C.O. Girit, J.C. Meyer, R. Erni, M.D. Rossell, C. Kisielowski, L. Yang, C. Park, M.F. Crommie, M.L. Cohen, Science 323 (2009) 17058.
[66] K. Nakada, M. Fujita, G. Dresselhaus, M.S. Dresselhaus, Phys. Rev. B 54 (1996) 17954.
[67] M. Fujita, K. Wakabayashi, K. Nakada, K. Kusakabe, J. Phys. Soc. Jpn. 65 (1996) 19203.
[68] F. Owens, Mol. Phys. 104 (2006) 31079.
[69] L. Yang, C. Park, Y. Son, M.L. Cohen, S.G. Louie, Phys. Rev. Lett. 99 (2007) 186801.
[70] V. Barone, O. Hod, G.E. Scuseria, Nano Lett. 6 (2006) 27484.
[71] X. Li, X. Wang, L. Zhang, S. Lee, H. Dai, Science 319 (2008) 12292.
[72] D. Finkenstadt, G. Pennington, M.J. Mehl, Phys. Rev. B 76 (2007) 121405.
[73] K. Lam, G. Liang, Appl. Phys. Lett. 92 (2008) 223106.
[74] B. Sahu, H. Min, A.H. MacDonald, S.K. Banerjee, Phys. Rev. B 78 (2008) 045404.
[75] D.W. Boukhvalov, M.I. Katsnelson, Phys. Rev. B 78 (2008) 085413.
[76] B. Huang, Z. Li, Z. Liu, G. Zhou, S. Hao, J. Wu, B. Gu, W. Duan, J. Phys. Chem. C 112 (2008) 1344246.
[77] E. Kan, Z. Li, J. Yang, J.G. Hou, J. Am. Chem. Soc. 130 (2008) 42245.
[78] Y. Guo, W. Guo, C. Chen, Appl. Phys. Lett. 92 (2008) 243101.
[79] L. Sun, Q. Li, H. Ren, H. Su, Q.W. Shi, J. Yang, J. Chem. Phys. 129 (2008) 074704.
[80] O. Hod, G.E. Scuseria, Nano Lett. 9 (2009) 26192.
[81] S. Costamagna, O. Hernandez, A. Dobry, Phys. Rev. B 81 (2010) 115421.
[82] S.M. Dubois, Z. Zanolli, X. Declerck, J.C. Charlier, Eur. Phys. J. B: Condens. Matter Complex Syst. 72 (2009) 1.
[83] Y. Son, M.L. Cohen, S.G. Louie, Phys. Rev. Lett. 97 (2006) 216803804.
[84] Y. Son, M.L. Cohen, S.G. Louie, Nature 444 (2006) 347.
[85] H. Lee, Y. Son, N. Park, S. Han, J. Yu, Phys. Rev. B 72 (2005) 174431.
[86] H. Murayama, T. Maeda, Nature 345 (1990) 791.
[87] J. Campos-Delgado, Y. Kim, T. Hayashi, A. Morelos-Gómez, M. Hofmann, H. Muramatsu, M. Endo, H. Terrones, R. Shull, M.S. Dresselhaus, M. Terrones, Chem. Phys. Lett. 469 (2009) 177.
[88] Y. Okuno, T. Ohba, H. Kanoh, K. Kaneko, M. Endo, H. Terrones, M.S. Dresselhaus, M. Terrones, J. Campos-Delgado, J.M. Romo-Herrera, X. Jia, D.A. Cullen, H. Muramatsu, Y.A. Kim, T. Hayashi, Z. Ren, D.J. Smith, Nano Lett. 8 (2008) 27738.
[89] P. Mahanandia, K. Nanda, V. Prasad, S. Subramanyam, Mater. Res. Bull. 43 (2008) 32522.
[90] J. Vaari, J. Lahtinen, P. Hautojärvi, Catal. Lett. 44 (1997) 43.
[91] P.W. Sutter, J. Flege, E.A. Sutter, Nat. Mater. 7 (2008) 406.
[92] X. Li, W. Cai, J. An, S. Kim, J. Nah, D. Yang, R. Piner, A. Velamakanni, I. Jung, E. Tutuc, S.K. Banerjee, L. Colombo, R.S. Ruoff, Science 324 (2009) 13124.
[93] A. Reina, S. Thiele, X. Jia, S. Bhaviripudi, M.S. Dresselhaus, J.A. Schaefer, J. Kong, Nano Res. 2 (2010) 509.
[94] D. Wei, Y. Liu, H. Zhang, L. Huang, B. Wu, J. Chen, G. Yu, J. Am. Chem. Soc. 131 (2009) 1114754.

[95] L.G. Cançado, M.A. Pimenta, B.R.A. Neves, G. Medeiros-Ribeiro, T. Enoki, Y. Kobayashi, K. Takai, K. Fukui, M.S. Dresselhaus, R. Saito, A. Jorio, Phys. Rev. Lett. 93 (2004) 047403.
[96] X. Yang, X. Dou, A. Rouhanipour, L. Zhi, H.J. Rader, K. Mullen, J. Am. Chem. Soc. 130 (2008) 42167.
[97] Y. Xiong, Y. Xie, X. Li, Z. Li, Carbon 42 (2004) 14473.
[98] Z. Kang, E. Wang, B. Mao, Z. Su, L. Gao, S. Lian, L. Xu, J. Am. Chem. Soc. 127 (2005) 65345.
[99] N.G. Chopra, L.X. Benedict, V.H. Crespi, M.L. Cohen, S.G. Louie, A. Zettl, Nature 377 (1995) 135.
[100] M. Yu, O. Lourie, M.J. Dyer, K. Moloni, T.F. Kelly, R.S. Ruoff, Science 287 (2000) 637.
[101] H.R. Gutiérrez, U.J. Kim, J.P. Kim, P.C. Eklund, Nano Lett. 5 (2005) 21951.
[102] C. Lin, T. Chen, T. Chin, C. Lee, H. Chiu, Carbon 46 (2008) 741.
[103] M. Motta, A. Moisala, I. Kinloch, A. Windle, Adv. Mater. 19 (2007) 37216.
[104] A.G. Cano-Márquez, F.J. Rodríguez-Macías, J. Campos-Delgado, C.G. Espinosa-González, F. Tristán-Loĭpez, D. Ramírez-González, D.A. Cullen, D.J. Smith, M. Terrones, Y.I. Vega-Cantú, Nano Lett. 9 (2009) 15273.
[105] D.V. Kosynkin, A.L. Higginbotham, A. Sinitskii, J.R. Lomeda, A. Dimiev, B.K. Price, J.M. Tour, Nature 458 (2009) 872.
[106] L. Jiao, L. Zhang, X. Wang, G. Diankov, H. Dai, Nature 458 (2009) 877.
[107] M. Terrones, Nature 458 (2009) 845.
[108] A.L. Elías, A.R. Botello-Méndez, D. Meneses-Rodríguez, V.J. González, D. Ramírez-González, L. Ci, E. Muñoz-Sandoval, P.M. Ajayan, H. Terrones, M. Terrones, Nano Lett. 9 (2009) 31371.
[109] K. Kim, A. Sussman, A. Zettl, ACS Nano 4 (2010) 13626.
[110] H. Santos, L. Chico, L. Brey, Phys. Rev. Lett. 103 (2009) 086801.
[111] A.L. Higginbotham, D.V. Kosynkin, A. Sinitskii, Z. Sun, J.M. Tour, ACS Nano 4 (2010) 20599.
[112] L. Jiao, X. Wang, G. Diankov, H. Wang, H. Dai, Nat. Nano 5 (2010) 321.
[113] L. Ci, Z. Xu, L. Wang, W. Gao, F. Ding, K. Kelly, B. Yakobson, P. Ajayan, Nano Res. 1 (2008) 116.
[114] S.S. Datta, D.R. Strachan, S.M. Khamis, A.T.C. Johnson, Nano Lett. 8 (2008) 19125.
[115] L.C. Campos, V.R. Manfrinato, J.D. Sanchez-Yamagishi, J. Kong, P. Jarillo-Herrero, Nano Lett. 9 (2009) 26004.
[116] R. Baker, R. Sherwood, E. Derouane, J. Catal. 75 (1982) 382.
[117] S. Trasobares, C. Ewels, J. Birrell, O. Stephan, B. Wei, J. Carlisle, D. Miller, P. Keblinski, P. Ajayan, Adv. Mater. 16 (2004) 610.
[118] M. Zhang, D.H. Wu, C.L. Xu, Y.F. Xu, W.K. Wang, Nanostruct. Mater. 10 (1998) 11452.
[119] R.L. McCarley, S.A. Hendricks, A.J. Bard, J. Phys. Chem. 96 (1992) 1008992.
[120] M. Moreno-Moreno, A. Castellanos-Gomez, G. Rubio-Bollinger, J. Gomez-Herrero, N. Agraït, Small 5 (2009) 924.
[121] F. Banhart, Rep. Progr. Phys. 62 (1999) 11811.
[122] A.V. Krasheninnikov, F. Banhart, Nat. Mater. 6 (2007) 723.
[123] H. Duan, E. Xie, L. Han, Z. Xu, Adv. Mater. 20 (2008) 32848.
[124] L. Tapaszto, G. Dobrik, P. Lambin, L.P. Biro, Nat. Nano 3 (2008) 397.
[125] L.P. Biró, P. Lambin, Carbon 48 (2010) 26779.
[126] T.G. Pedersen, C. Flindt, J. Pedersen, N.A. Mortensen, A. Jauho, K. Pedersen, Phys. Rev. Lett. 100 (2008) 136804814.
[127] A. Stone, D. Wales, Chem. Phys. Lett. 128 (1986) 501.
[128] P.A. Thrower, Chem. Phys. Carbon 5 (1969) 217.
[129] M. Terrones, G. Terrones, H. Terrones, Struct. Chem. 13 (2002) 373.
[130] M. Terrones, H. Terrones, Fuel Energy Abstr. 37 (1996) 269.
[131] A.R. Botello-Méndez, F. López-Urías, E. Cruz-Silva, B.G. Sumpter, V. Meunier, M. Terrones, H. Terrones, Phys. Stat. Solidi (RRL)-Rapid Res. Lett. 3 (2009) 181.
[132] M.S. Dresselhaus, M. Terrones, A. Jorio, M. Endo, A. Rao, Y. Kim, T. Hayashi, H. Terrones, J. Charlier, G. Dresselhaus, Mater. Today 7 (2004) 30.
[133] J. Campos-Delgado, I.O. Maciel, D.A. Cullen, D.J. Smith, A. Jorio, M.A. Pimenta, H. Terrones, M. Terrones, ACS Nano 4 (2010) 16962.
[134] E. Cruz-Silva, F. López-Urías, E. Muñoz-Sandoval, B.G. Sumpter, H. Terrones, J.C. Charlier, V. Meunier, M. Terrones, ACS Nano 3 (2009) 19131.
[135] M. Terrones, A. Jorio, I.O. Maciel, J. Campos-Delgado, E. Cruz-Silva, M.A. Pimenta, B.G. Sumpter, V. Meunier, F. López-Urías, E. Muñoz-Sandoval, H. Terrones, Nano Lett. 9 (2009) 22672.
[136] L. Novotny, A. Jorio, I.O. Maciel, N. Anderson, M.A. Pimenta, A. Hartschuh, H. Qian, M. Terrones, H. Terrones, J. Campos-Delgado, A.M. Rao, Nat. Mater. 7 (2008) 878.
[137] M. Terrones, F. Banhart, N. Grobert, J.C. Charlier, H. Terrones, P.M. Ajayan, Phys. Rev. Lett. 89 (2002) 075505.
[138] M. Terrones, H. Terrones, F. Banhart, J.C. Charlier, P.M. Ajayan, Science 288 (2000) 12269.
[139] M. Endo, B.J. Lee, Y.A. Kim, Y.J. Kim, H. Muramatsu, T. Yanagisawa, T. Hayashi, M. Terrones, M.S. Dresselhaus, New J. Phys. 5 (2003) 1211.
[140] W. Bao, F. Miao, Z. Chen, H. Zhang, W. Jang, C. Dames, C.N. Lau, Nat. Nanotechnol. 4 (2009) 562.
[141] Z. Li, Z. Cheng, R. Wang, Q. Li, Y. Fang, Nano Lett. 9 (2009) 35992.
[142] F. Cervantes-Sodi, G. Csanyi, S. Piscanec, A.C. Ferrari, Phys. Rev. B 77 (2008) 165427513.
[143] S. Yu, W. Zheng, Q. Wen, Q. Jiang, Carbon 46 (2008) 537.
[144] B. Biel, F. Triozon, X. Blase, S. Roche, Nano Lett. 9 (2009) 27259.
[145] D. Wei, Y. Liu, Y. Wang, H. Zhang, L. Huang, G. Yu, Nano Lett. 9 (2009) 17528.
[146] X. Wang, X. Li, L. Zhang, Y. Yoon, P.K. Weber, H. Wang, J. Guo, H. Dai, Science 324 (2009) 768.
[147] A.C. Ferrari, J.C. Meyer, V. Scardaci, C. Casiraghi, M. Lazzeri, F. Mauri, S. Piscanec, D. Jiang, K.S. Novoselov, S. Roth, A.K. Geim, Phys. Rev. Lett. 97 (2006) 187401.
[148] L. Malard, M.A. Pimenta, G. Dresselhaus, M.S. Dresselhaus, Phys. Rep. 473 (2009) 51.
[149] P. Poncharal, A. Ayari, T. Michel, J. Sauvajol, Phys. Rev. B 78 (2008) 113407.
[150] C. Chen, W. Bao, J. Theiss, C. Dames, C.N. Lau, S.B. Cronin, Nano Lett. 9 (2009) 41726.
[151] L.M. Malard, D.C. Elias, E.S. Alves, M.A. Pimenta, Phys. Rev. Lett. 101 (2008) 257401.
[152] L.M. Beltrán del Río, A. Gómez, SimulaTem, alfredo@fisica.unam.mx, n.d.
[153] J. Lahiri, Y. Lin, P. Bozkurt, I.I. Oleynik, M. Batzill, Nat. Nano 5 (2010) 326.
[154] R. Sordan, F. Traversi, V. Russo, Appl. Phys. Lett. 94 (2009) 073305.
[155] Y. Lin, C. Dimitrakopoulos, K.A. Jenkins, D.B. Farmer, H. Chiu, A. Grill, P. Avouris, Science 327 (2010) 662.
[156] J.C. Meyer, C.O. Girit, M.F. Crommie, A. Zettl, Nature 454 (2008) 319.
[157] Z. Lee, K. Jeon, A. Dato, R. Erni, T.J. Richardson, M. Frenklach, V. Radmilovic, Nano Lett. 9 (2009) 33659.
[158] R. Petersen, T.G. Pedersen, Phys. Rev. B 80 (2009) 113404414.
[159] J.A. Furst, T.G. Pedersen, M. Brandbyge, A. Jauho, Phys. Rev. B 80 (2009) 115117126.
[160] D. Jiang, V.R. Cooper, S. Dai, Nano Lett. 9 (2009) 40194.

[161] H. Terrones, Y. Bando, D. Golberg, M. Terrones, J.C. Charlier, A. Gloter, E. Cruz-Silva, E. Terrés, Y.B. Li, A. Vinu, Z. Zanolli, J.M. Dominguez, Nano Lett. 8 (2008) 10262.
[162] L. Ci, L. Song, C. Jin, D. Jariwala, D. Wu, Y. Li, A. Srivastava, Z.F. Wang, K. Storr, L. Balicas, F. Liu, P.M. Ajayan, Nat. Mater. 9 (2010) 430.
[163] A.R. Botello-Méndez, F. López-Urías, M. Terrones, H. Terrones, Nano Lett. 8 (2008) 15625.
[164] A. Botello-Méndez, F. López-Urías, M. Terrones, H. Terrones, Nano Res. 1 (2008) 420.
[165] A.R. Botello-Méndez, F. López-Urías, M. Terrones, H. Terrones, Nanotechnology 20 (2009) 325703.

Mauricio Terrones obtained his B.Sc. degree in Engineering Physics with first class honours at Universidad Iberoamericana, and was distinguished as the Best Student of Mexico in Engineering Physics in 1992. In 1994 he started his doctorate degree with Sir Prof. Harold W. Kroto (Nobel Laureate, FRS) and received his D.Phil. degree from University of Sussex in 1997. He has co-authored more than 270 publications in international journals, and counts with more than 9000 citations to his work (His H index is 52). He has numerous awards including: the Alexander von Humboldt Fellowship, the Mexican National Prize for Chemistry, the Javed Husain Prize and the Albert Einstein medal from UNESCO, the TWAS Prize in Engineering Physics, the Carbon Prize given by the Japanese Carbon Society, the Somiya Award by the International Union of Materials Research Societies, among others. Aged 41, he currently holds a chair of excellence at Universidad Carlos III of Madrid, and he was the pioneer of the National Laboratory for Nanoscience and Nanotechnology Research (LINAN) at IPICYT in Mexico. His research now concentrates on the theory, synthesis and characterization of novel layered nanomaterials, including graphene, and he will join Shinshu University (Japan), as outstanding professor, from August 2010.

Andrés R. Botello-Méndez received his BS in Physics Engineering in 2004 from ITESM (Mexico), and his PhD in Applied Sciences (Nanoscience and Nanotechnology) in 2009 from IPICYT (Mexico). He has worked in the study of the electronic properties of ZnO and carbon nanostructures. He is mainly involved in theoretical and experimental studies of the properties of one-dimensional nanostructures from layered compounds. Presently, he is doing a postdoctoral stay at the Institute of Condensed Matter and Nanosciences (ICMN) of the Catholic University of Louvain in Belgium were he obtained the Marcel de Merre Prize of Louvain.

Jessica Campos-Delgado received her B.S. in Physics Engineering from the State University of San Luis Potosi, Mexico in 2005. She enrolled the graduated program of Applied Sciences at the Institute of Science and Technology of San Luis Potosi in Mexico and obtained her PhD degree in 2009. She is currently working as a Post-Doc at the National Institute of Metrology, Standardization and Industrial Quality of Brazil. Her research interests are towards the synthesis of carbon nanostructures and their characterization through Raman spectroscopy and electron microscopy.

Florentino López-Urías carried out his BSc degree in Physical Sciences at the Autonomous University of Sinaloa (México). He pursued his MSc. in Physical Sciences at the Autonomous University of San Luis Potosí (México), and received the PhD degree in Physics from the University Paul Sabatier in Toulouse (France). His research interests include theoretical and experimental aspects of graphene materials as well as diverse magnetic nanostructures.

Yadira I. Vega-Cantú received her Ph.D. from Rice University (USA) in 2002, where she worked in Professor W. Edward Billups research group. Her thesis work, received the Harry B. Weiser Award, and her postdoctoral stay dealt with industrial projects. Currently, she is a Professor in the Nanoscience and Nanotechnology program at the Advanced Materials Department at IPICYT. She currently advises eight graduate students. Her research interests include chemistry of carbon nanotubes, carbon nanoribbons and graphene, characterization and processing of polymer nanocomposites and development of applications such as actuators and sensors.

Fernando J. Rodríguez-Macías has a B.S. (Chemistry, with honours) from ITESM (México). He worked on carbon nanotubes with Professor Richard E. Smalley at Rice University (USA) during his M.A. (1999). He participated in interdisciplinary research in Materials Science at Rice for his Ph.D. (Chemistry, 2004) and a postdoctoral stay with Professor Enrique V. Barrera, producing a patent and papers related to nanotube composites. He joined IPICYT in 2005 and he is currently a Professor in the Nanoscience and Nanotechnology program, advising five graduate students. His research interests include composites of nanocarbons and their chemical modification to control the interface, doped-carbon nanotubes, graphene, biocompatibility of nanomaterials and bionanotechnology.

Ana Laura Elías received her Ph.D. degree in Nanoscience and Nanotechnology from IPICyT (México) in 2006. She has a Physics background, form her undergraduate degree (UASLP-Mexico, 2002). Ana Laura has visited several institutions for research stays, such as LANL (in New Mexico, USA), MIT (Cambridge, MA), ASU (Tempe, AZ), UNAM (Mexico City), Rice University (Houston, TX) and RPI (Troy, NY). She was a postdoctoral research fellow at Shinshu University (Japan), in the group of Prof. Morinobu Endo and at IPICyT (Mexico). Currently, she is a postdoctoral research fellow at Rice University, in Prof. Ajayan's group (since June 2009).

Emilio Muñoz-Sandoval obtained his PhD in Physics from the Universidad Autónoma de San Luis Potosí (México), and carried out postdoctoral stays at UNAM (México) and the Netherlands. His current research deals with production and characterization of different carbon nanomaterials and ferromagnetic nanoparticles encapsulated in carbon nanostructures. During the 9 years, working with Professors Terrones and collaborators Emilio has acquired invaluable experimental expertise by evolving a multidisciplinary approach combining the production of nanomaterials with electron microscopy and magnetometry techniques for analysis. In order to control the size and morphology, he has developed several routes to deposit catalytic nanoparticles. Magnetron sputtering deposition has been the most successful method to achieve these goals.

Abraham G. Cano-Márquez got a Bachelor's diploma in Chemistry at the Universidad Autonoma de San Luis Potosí (México), whence he also received a master's degree in Physical Chemistry after studying the electromicrogravimetric behaviour of a sulfonated polyaniline. He will soon finish his PhD studies at IPICYT (México). His research interests are the development of carbon-based nanostructures, focusing in the study of graphene-like materials and devices. He is also interested in the study of polyanilines and their composites with carbon materials for the development of new actuators for use in robotics and prosthetics. He is part of the team that introduced the exfoliation technique for the unzipping of multi-walled carbon nanotubes.

Jean-Christophe Charlier is Professor at the Institute of Condensed Matter and Nanosciences of the University of Louvain (UCL) and Senior Research Associate of the Fund for Scientific Research (FNRS) in Belgium. His research interests are in theoretical condensed matter physics and nanosciences covering the areas of: electronic and structural properties of crystals and reduced-dimensional solids; nanotubes, graphene and related carbon-based nanostructures; quantum transport through single molecules and other nanosystems. The objective is to explain and predict the properties of materials using first-principles theories and computational physics. He is author of about hundred scientific publications in international peer-reviewed journals.

Humberto Terrones obtained his PhD degree from Birkbeck College in 1992 (University of London) under the supervision of Prof. Alan L. Mackay (FRS). Following a postdoctoral stay at Cambridge University (UK), Humberto joined the Institute of Physics at (UNAM) in Mexico City. He then moved to IPICYT as Head of the Advanced Materials Department, to work mainly in nanosciences and nanotechnology introducing a multidisciplinary character to research. He is presently visiting Professor at the Institute of Condensed Matter and Nanosciences of the Université Catholique de Louvain in Belgium. Alan L. Mackay and HumbertoTerrones were the first to introduce the concept of curvature in layered materials to understand and propose new nanostructures.